KINETICS OF INFLUENZA A VIRUS INFECTIONS IN A HETEROGENEOUS CELL POPULATION

by

Marc J. Baron

B.Sc (Hons.), University of Saskatchewan, Saskatoon, SK, Canada, 2008

A thesis

presented to Ryerson University

in partial fulfillment of the

requirements for the degree of

Master of Science

in the Program of

Biomedical Physics

Toronto, Ontario, Canada, 2009

AUTHOR DECLARATION

I hereby declare that I am the sole author of this thesis.

I authorize Ryerson University to lend this thesis to other institutions or individuals for the purpose of scholarly research.

_____

Marc J. Baron

I further authorize Ryerson University to reproduce this thesis by photocopying or by other means, in total or in part, at the request of other institutions or individuals for the purpose of scholarly research.

_____

Marc J. Baron

ABSTRACT

KINETICS OF INFLUENZA A VIRUS INFECTIONS IN A HETEROGENEOUS CELL POPULATION

Marc J. Baron

Master of Science, Biomedical Physics

Ryerson University, 2009

Several mechanisms have been proposed to account for the marked increase in severity of human infections with avian influenza compared to human influenza strains, including increased cytokine expression, poor immune response, and differences in target cell receptor affinity. Here, the effect of target cell tropism on disease severity is studied using a mathematical model for in-host influenza viral infection in a cell population consisting of two different cell types. The two cell types differ only in their susceptibility to infection and rate of viral production. We show the existence of a parameter regime which is characterized by high viral loads sustained long after the onset of infection. This finding suggests that cell tropism alone is sufficient to explain the increase in infection severity of certain strains of the influenza A virus. The implications of this finding for antiviral treatment strategies will be discussed.

ACKNOWLEDGMENTS

Many people have contributed to my work here at Ryerson University. First I thank my supervisor Dr. Catherine Beauchemin for guiding my research, as well as providing many helpful suggestions throughout my time here. I thank the members of my supervisory committee, Dr. Katrin Rohlf and Dr. J. Carl Kumaradas, who provided helpful guidance during our meetings, and Dr. Nancy Ford, who agreed to sit on my examination committee. I would like to acknowledge Dr. Benjamin Holder and Dr. Hana Dobrovolny for helpful discussions during the course of this research, as well as the support staff in the Department of Physics at Ryerson University for help in various capacities. I would like to acknowledge the Natural Sciences and Engineering Research Council for providing funding for this work, and Ryerson University for financial assistance.

Lastly, I would like to thank my family for moral support.

Contents

List of Tables

List of Figures

Chapter 1

Introduction

Influenza is a widespread virus which infects cells in the respiratory tract. Annual influenza outbreaks result in the deaths of hundreds of thousands of people worldwide [90], and this number may increase substantially for outbreaks of pandemic influenza. The most well-known influenza pandemic is the 1918 Spanish influenza outbreak, where an estimated 50 million people succumbed to infection, approximately 3% of the world's population at the time [40]. In recent years, attention has focused on the avian-derived influenza A (H5N1) virus strain, which has the potential to evolve into a pandemic viral strain [62]. More recently, the swine-origin influenza A (H1N1) strain, which is responsible for the current influenza pandemic, has been a cause for concern, given the strain's ability to cause severe illness [59].

Several biological techniques have been employed in order to gain insight into the causes of influenza infection severity, including in vitro studies in cell cultures, in vivo animal studies and data gathered from viral infections in humans. Mathematical modelling has been used as a tool to extract further information about influenza infections gathered from biological data. By creating models which incorporate the mechanisms of infection, a better understanding of the mechanisms at play and their role in shaping the dynamics of the infection can be acquired. In some cases, one can uncover novel behaviours which can then

be tested experimentally.

Although a wide body of knowledge exists for the study of novel, highly virulent influenza viruses, the reasons for the severity of these viruses are not well understood. In particular, while mathematical models have been developed to study the within-host dynamics of seasonal influenza viruses [1, 5, 31, 32, 46], no models have attempted to explain the underlying mechanisms which can bring about an increase in disease severity in some viral strains.

In this thesis, mathematical modelling is used to explore the effect of influenza infection within a population of cells containing two different types of cells. In Chapter 2, the biology of the influenza A virus will be discussed, including highly virulent influenza strains, such as the H5N1 strain, and the potential role differential cell tropism plays in disease severity.

Chapter 3 follows with a review of mathematical modelling in the study of within-host viral infections, including influenza, as well as a discussion on data fitting. In Chapter 4, we use a mathematical model to test the hypothesis that cell tropism is sufficient to explain the increased severity of infection caused by certain strains of the influenza virus. It is shown that this model can lead to long-lasting influenza infections characterised by high viral loads. This will be justified through the use of a theoretical analysis, as well as with experimental data.

The analysis is continued in Chapter 5, where the parameters of the model are rescaled to study how this change in parameters affects the progression of viral infection. A summary of the overall work, as well as potential implications for future studies, follows in Chapter 6.

Chapter 2

Biology of influenza A virus

The influenza A virus is a member of the Orthomyxoviridae family, which also includes the influenza B and C viruses. The influenza A genus is considered to be the most severe of the influenza genera, as the four influenza pandemics of the past 100 years have all been influenza A viruses. Influenza A viruses are further categorized by the antibody response elicited against the virus [90]. This response is determined by two virus surface proteins: haemagglutinin (H) and neuraminidase (N). Influenza A sub-types are named after these surface proteins, e.g. Influenza A (H1N1).

Infection is initiated by virus particles, or virions, which infect susceptible cells in the respiratory tract. Virions bind to receptors on the surface of a susceptible cell, and are absorbed into the cell through endocytosis. Once inside, the viral genetic material is released and transported to the cell nucleus. Copies of the viral genome are produced and used to hijack the "machinery" of the cell, causing the cell to start producing viral proteins. The viral proteins, along with the virus' genetic material, are assembled within the cell. After an initial delay, virions are released from the infected cell, where they are free to infect other susceptible cells. After an initial delay, influenza virions are released continuously until the cell ceases production or is destroyed by immune effects.

The influenza virus is an RNA virus, with a genome segmented into 8 separate strands

which encode for the different viral proteins [10]. Changes to the virus genome, which may result in greater infection severity, occur in one of two main ways: antigenic drift and antigenic shift. In antigenic drift, small changes to viral antigens through mutations allow the virus to slowly evade immunological memory, resulting in a less rapid secondary immune response. Unlike DNA, RNA lacks any proof-reading mechanisms during replication, resulting in a high rate of mutation, approximately 1 per genome per replication for RNA viruses such as influenza [21]. Antigenic drift occurs gradually, as there are a large number of genetic mutations which can take place and only a few of them may lead to beneficial effects. On the other hand, antigenic shift occurs when the segmented genetic material from different viral strains combine in a newly formed influenza virion, leading to the creation of a novel strain. In the past, novel influenza viruses produced through these mechanisms have led to highly virulent strains and global pandemics [40]. As a result of these possible changes, influenza is a great public health concern.

2.1 Infection dynamics

The influenza virus is transmitted between hosts primarily through the inhalation of aerosols containing the influenza virus, which is expelled from the infected host by coughing or sneezing, though it can also enter through direct contact of the virus with the eyes, mouth or nose [29]. The virus infects epithelial cells lining the respiratory tract by binding to receptors expressed on the surface of these cells. Viral proteins and genetic material is then produced within the infected cells, and virions are released 4–8 h after infection [1], at a rate of 10^2–10^4 d^{-1} in the respiratory tract [6]. Biological estimates suggest an average lifetime of 12–24 h for infected cells [1, 6].

Influenza viral infections are characterized by rapid initial growth of the infection, and a relatively short duration. The viral titer[1] generally peaks 2–3 days post-infection (dpi) and is

[1]Viral titer is an experimental measure of the concentration of virus in a sample collected from an infected

cleared 6–8 dpi [1,6]. Influenza viral infections are also characterized by rapid degeneration of the epithelial cell population. Clinical symptoms usually manifest after 10% of the epithelial cells in the upper airways are damaged, and at the peak of infection, 30-50% of these cells are destroyed [6].

Currently, the relationship between level of viral titer and the development of symptoms is not well established. The development of symptoms does not depend solely on the level of viral titer, but also the immune response of the individual to infection, which may be highly variable. In addition, certain experimental techniques for measuring viral load may not discern between infectious and non-infectious virus. Therefore, there may not be a straightforward correlation between the onset of symptoms and quantitative measures of viral titer.

However, the onset of symptoms for human-derived influenza strains occurs around 1-2 dpi, and dissipates around 5-6 dpi [24, 33]. These time points correspond to times when the viral titer surpasses 10^4 $TCID_{50}$ in experimental infections [1]. This may provide an estimate as to what level of viral titer corresponds to the development of symptoms in infected individuals.

2.2 Immune response

The body's ability to elicit a rapid immune response is important for reducing the severity of viral and bacterial infections. In order to fight the large variety of pathogens that the body encounters, the immune system has a wide range of responses, acting over different time scales. The immune system is categorized into two major components: non-specific and specific responses.

The first non-specific response a foreign pathogen encounters are physical barriers, such as hair, skin and mucus. If physical barriers do not prevent the pathogen from entering the body,

individual or cell culture system.

responses from within the body are triggered. These innate (or non-specific) responses are triggered when a pathogen encounters a phagocytic cell (e.g. macrophage, natural killer cell), which engulfs the pathogen and releases proteins called cytokines. Cytokines are chemical signals emitted by some cells which trigger other phagocytic cells to descend upon the area of infection, which in turn release their own cytokines, resulting in a cascade of immune cells. As the name suggests, the innate response is non-specific, meaning that pathogens are cleared in a generic way and no long-lasting immunity is conferred through this process. However, pathogens may bypass the innate response, in which case the more specific adaptive immune response is triggered within the body.

The adaptive immune system offers a more complex and specific response to encounters with a pathogen. The adaptive system is characterised by the recognition of specific molecules on foreign pathogens called antigens, which leads to long-lasting immunological memory against these molecules. Differentiated white blood cells called lymphocytes are the main components of the adaptive immune system. These lymphocytes can be further split into two major categories: the humoral response (mediated by lymphocytes called B cells) and the cell-mediated immune response (mediated by lymphocytes called T cells). The cell-mediated response consists of two main types of cells called cytotoxic T lymphocytes (CTLs) and helper T cells (T_H cells). CTLs recognise specific antigens on the surface of infected cells and subsequently eliminate those cells, while helper T cells release cytokines which signal phagocytic cells and stimulate CTLs into action, and differentiate into memory T cells, which provide long-lasting recognition of specific antigens. T_H cells are also responsible for activating B cells, which mediate the humoral response. Activated B cells differentiate into plasma cells, which release millions of proteins called antibodies, which help identify and neutralize foreign pathogens, and memory B cells, which, along with memory T cells, are responsible for conferring long-lasting immunity to specific pathogens. A graphical summary of the adaptive immune response is shown in Figure 2.1.

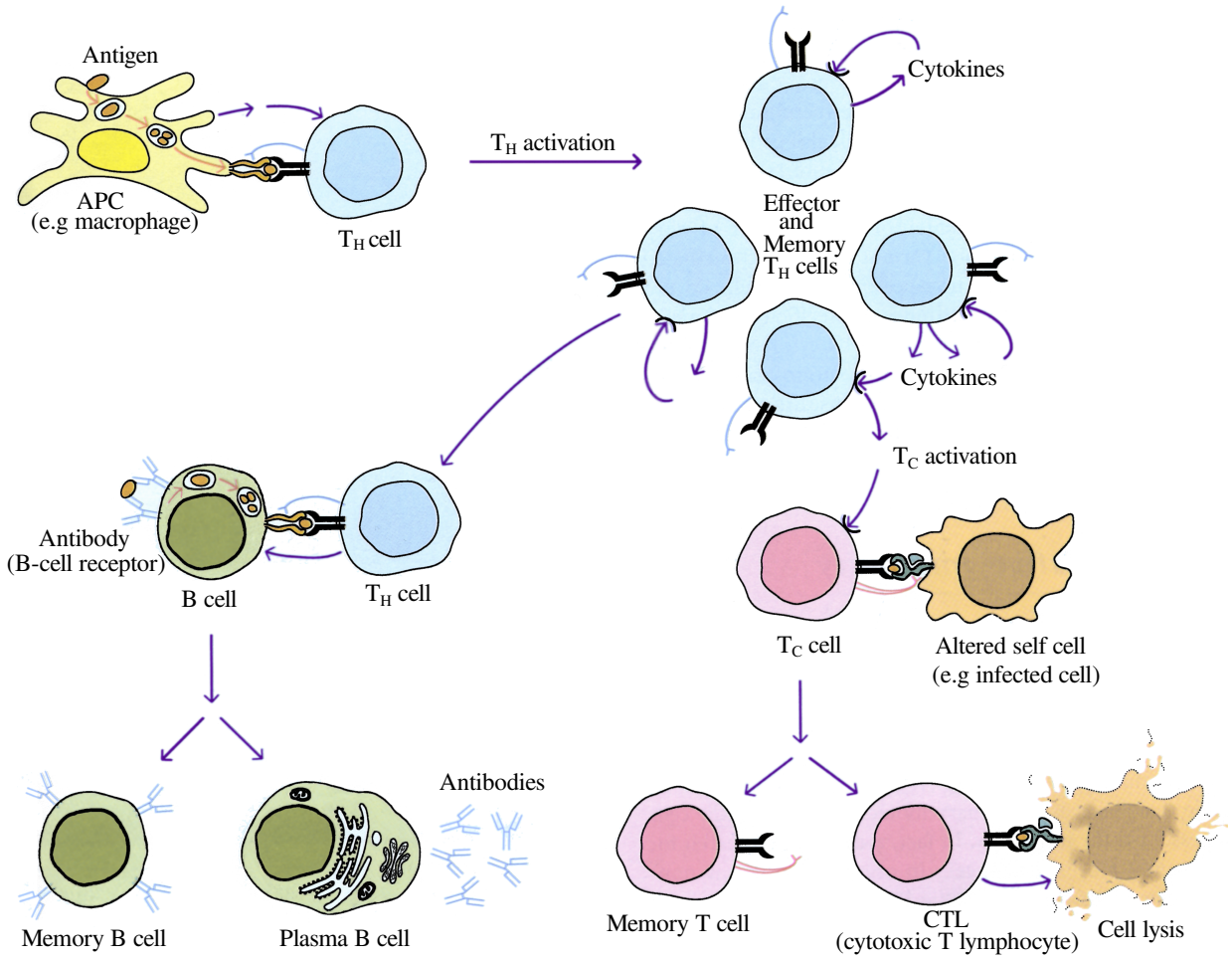

Figure 2.1 Representation of adaptive immune system. Graphical summary of the adaptive immune response to a foreign antigen. Antigen-presenting cells (APC) activate T helper cells (T_H cell), as shown at the top of the figure. T_H cells activate the antibody-mediated response, which leads to the release of proteins called antibodies (left hand side) which neutralize the foreign pathogen. T helper cells, in conjunction with infected cells, also activate the cytotoxic immune response, which results in the elimination of infected cells (right hand side). Both processes lead to the development of long-term immunological memory against the specific pathogen. Figure adapted from [28] .

Due to the relatively short duration of influenza infection, the early, innate immune responses play a primary role in clearing the infection. Various cytokines become elevated early after infection is initiated, and peak at approximately the same time as the viral titer, while elements of the adaptive immune response do not begin to increase until after peak viral replication [1].

2.3 Highly virulent influenza viruses

On occasion, a novel influenza originating in an animal host may enter a human population. While the strain may be mild in its natural animal host, it can be highly virulent in a human host, i.e., it will have the ability to cause severe illness and spread efficiently through the population. When an infectious disease meets these requirements, it is known as a pandemic. The worldwide death toll may increase substantially for pandemic influenza strains, and the H5N1 and H1N1 strains have recently garnered attention for their potential to evolve into widespread, highly virulent strains.

The difference in virulence between different strains of influenza has not been readily explained. Possible explanations for these differences include an increased level of cytokine production, a poor immune response to the strain's novelty, and differences in a strain's particular affinity for the receptors expressed on the surface of various susceptible cells populating the host's airways. These explanations will be discussed in the following sections.

2.3.1 Immune response

Infection with influenza A (H5N1) is associated with elevated levels of proinflammatory cytokines. In patients infected with influenza strains with low pathogenicity, the level of specific cytokines is generally associated with the development of symptoms [41]. In studies of patients infected with influenza A (H5N1), high viral loads and elevated levels of

proinflammatory cytokines have been found [16], and post-mortem analysis of patients who succumbed to infection were found to have high levels of macrophages and lymphocytes in the lungs, as well as significant tissue damage [67, 83].

Similar results were found during in vitro studies of viral infection. When human primary alveolar and bronchial epithelial cells were infected with influenza A (H5N1), a much greater number of proinflammatory cytokines were induced than infection from human-derived influenza strains [8]. Similarly, infecting human primary monocyte-derived macrophages in vitro with influenza A (H5N1) led to much higher induction of proinflammatory cytokines than for infection with human-derived influenza strains [9]. In both cases, similar levels of virus were produced by the avian-derived and human-derived influenza strains, suggesting the induction of increased levels of proinflammatory cytokines may not necessarily be caused by high levels of viral titer.

It is not clear whether the high mortality associated with influenza A (H5N1) infections is due to the massive induction of proinflammatory cytokines, or if this is a byproduct of the high levels of virus produced during these more severe infections. Some studies have suggested that the elevated immune response may be due to the ability of influenza A (H5N1) to escape detection by the immune system. One study found that the ability of cytotoxic T cells to kill influenza A (H5N1) infected cells may be suppressed [38], suggesting that a change to the viral haemagglutinin protein may be responsible for the increased severity. A different study suggests that changes to the non-structural 1 (NS1) protein of the influenza virus may lead to resistance to the antiviral action of cytokines [77]. When the NS1 gene of a human influenza strain was replaced with that of an avian strain, a greater immune response was elicited from the new viral strain during infection in pigs. This suggests that the immune response cannot efficiently control infections by influenza A (H5N1). It is unclear, however, which, if any, of these mechanisms are primarily responsible for changes in virus level between strains.

2.3.2 Cell tropism

In order to infect a cell, influenza virions must successfully bind to epithelial cells in the respiratory tract. This is mediated by the influenza virus protein haemagglutinin (HA), which specifically binds to sialic acid receptors on the surface of the cell. The virus protein neuraminidase (NA) is also believed to play a role, though it is unclear what that role is or how the action is mediated [52, 54].

There are two specific surface cell receptors that are believed to be important for binding with the influenza virus: sialic acid α2,3 galactose terminated saccharides (SAα2,3 Gal) and sialic acid α2,6 galactose terminated saccharides (SAα2,6 Gal). These surface cell receptors are generally detected on different epithelial cells in the respiratory tract. Studies have found that SAα2,6 Gal surface receptors are predominantly (but not exclusively) expressed on non-ciliated, mucus-producing cells, while ciliated cells express both SAα2,3 Gal and SAα2,6 Gal receptors [39, 43, 82].

Different strains of influenza are believed to bind to different surface cell receptors. Studies have shown that human-derived virus strains appear to preferentially bind to SAα2,6 Gal surface cell receptors, expressed predominantly on non-ciliated cells, while avian-derived viruses seem to preferentially bind to SAα2,3 Gal surface cell receptors, expressed mainly on ciliated cells [51, 53, 79, 82]. This is illustrated in Figure 2.2(a). It is important to note that while a particular strain of influenza may preferentially bind to a certain type of cell, it will not necessarily bind exclusively to that cell type, as illustrated in Figure 2.2(b).

As mentioned, changes to the HA genetic sequence of an influenza virus can change its binding specificity for surface cell receptors. By changing a single amino acid in the HA protein of an influenza virus, the binding preference of human strains changes from SAα2,6 Gal (preferred by human-derived strains) to SAα2,3 Gal (preferred by avian-derived strains) [75]. This has been shown for different strains of human-derived influenza virus [69, 87] and this HA amino acid substitution is believed to increase the binding preference of avian-

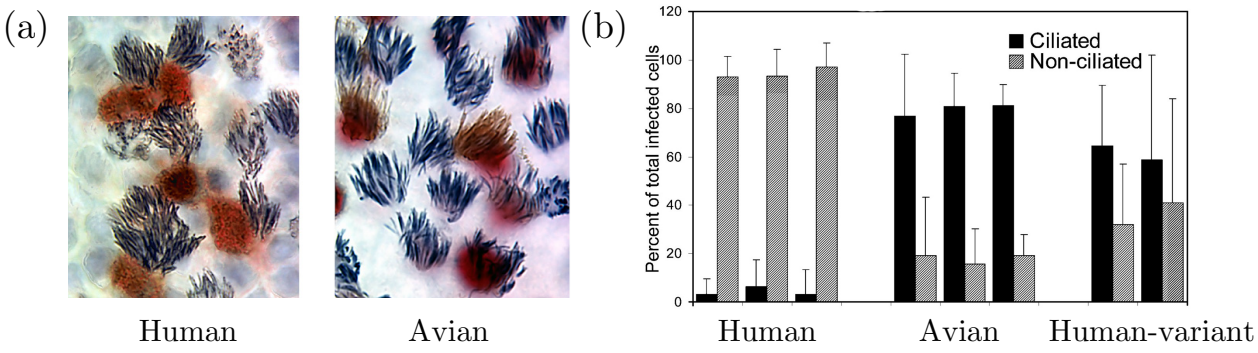

Figure 2.2 Cell tropism of influenza viruses. Influenza viruses exhibit cell tropism based on surface cell receptors. (a) Human-derived virus strains preferentially bind to non-ciliated cells, while avian-derived viruses bind mainly to ciliated cells. Immunostaining was performed for virus antigen (red) and cilia (blue). (b) Percentages of infected ciliated and non-ciliated cells for human and avian influenza strains, as well as a human strain with a single amino acid substitution which confers binding preferences similar to avian viral strains. All three images adapted from [51].

derived virus strains for SAα2,6 Gal receptors, and provide an increased affinity for spreading in humans [92].

It has also been suggested that sialic acid may not be the primary receptor for influenza virus infection. This was determined by treating human airway epithelial cells with the protein sialidase, which cleaves sialic acid receptors from the surface of the cell. After introducing different influenza viruses to these cells, it was found that some virus strains were able to successfully infect the cells despite their lack of sialic receptors [43, 58, 82]. This suggests the influenza virus may only temporarily bind to sialic acid surface receptors until a more specific receptor is located.

The distribution of surface cell receptors in the respiratory tract may be also be important when considering the ability of a virus strain to efficiently replicate, as the distribution of surface cell receptors appears to change in different regions of the respiratory tract. Specifically, SAα2,6 Gal receptors are dominantly expressed on cells in the upper respiratory tract, while SAα2,3 Gal receptors are detected at a much lower rate [43, 79]. On cells in the lower

respiratory tract, SAα2,3 Gal receptors were found to dominate [79]. Thus, the distribution of surface cell receptors in the respiratory tract may be one reason for the inability of certain influenza strains to efficiently replicate, as some influenza strains may not efficiently replicate in certain regions of the respiratory tract. However, changes to the HA protein of avian-derived strains may allow the virus to more easily spread throughout the respiratory tract, due to a change in receptor preference [53, 93]. Recent evidence suggests that the H1N1 pandemic strain may have the ability to efficiently replicate in the lower respiratory tract, possibly explaining the increased severity of this virus [11].

It is apparent from the various studies outlined that influenza virus cell tropism plays an important role in initiating viral infection. However, the role of cell tropism in the severity of the subsequent infection between different viral strains is currently not well understood.

2.3.3 Infection dynamics

At this time, most of the data for the dynamics of infection from highly virulent influenza viruses in humans comes from the influenza A (H5N1) avian-derived virus through clinical and experimental studies [63, 68]. Influenza A (H5N1) differs from more common strains in that infection is long-lasting, with high viral loads. In initial cases of infection, symptoms developed 2-4 days after exposure to infected poultry, while recent cases appear to have an incubation period as long as 8 days [63, 68]. Patients admitted to hospital showed typical symptoms associated with influenza virus infection. However, the infection rapidly spread to the lower respiratory tract, resulting in pneumonia and acute respiratory distress syndrome around 6-7 days after the onset of symptoms [12, 63]. Viral loads in patients infected with avian-derived influenza strains were also found to be 10 times higher than patients infected with human-derived strains [67]. Viral titer in patients infected with avian virus strains has been shown to peak approximately 5–6 dpi, compared to the 2–3 dpi for human virus strains [16]. The mortality rate among patients presenting infection with the influenza A

(H5N1) strains is 60% [89], with death occurring at a median time of 9 days after the onset of symptoms [12].

The recent outbreak of swine-origin influenza A virus (SOIV) pandemic strains may provide valuable data regarding the dynamics of pandemic influenza viral strains. However, due to the recent nature of the SOIV outbreak, data regarding the infection dynamics of the virus in humans is limited. Data culled from experimental infections in ferrets [50, 56], showed that viral titer peaked at higher levels for the novel SOIV than for seasonal influenza strains. The novel SOIV strains also spread more efficiently in the respiratory tract, with virus detected in the lungs of infected ferrets. The SOIV strains also caused increased morbidity compared to seasonal influenza virus strains in ferrets. Infection from the novel SOIV virus was found to last approximately 2 days longer than infections with seasonal strains, matching similar results from avian-origin influenza A (H5N1) infections. Therefore, it appears infections with highly virulent influenza strains are characterized by high viral loads which peak late and are sustained over extended periods compared to seasonal influenza strains.

Chapter 3

Mathematical models of virus dynamics

Mathematically, the analysis of viral infections in vivo is a specific case of modelling interacting populations. In the simplest model of an in-host virus infection, there are three populations to consider: uninfected target cells (which are susceptible to infection), infected cells and virions. When studying this basic system, we are primarily interested in how the system evolves over time; ordinary differential equations (ODEs) are therefore used for this purpose. Other methods have been considered, including cellular automaton [95] and agent-based models [3]; however, ODE models are more commonly used due to their simplicity and well-characterized behaviour.

The basic model of virus dynamics can be written as follows [7, 60, 70]:

$$\begin{aligned} \frac{\mathrm{d}T}{\mathrm{d}t} &= -\beta TV \\ \frac{\mathrm{d}I}{\mathrm{d}t} &= \beta TV - \delta I \\ \frac{\mathrm{d}V}{\mathrm{d}t} &= pI - cV \ . \end{aligned} \tag{3.1}$$

Susceptible cells, T, can be infected by virus, V, becoming infected cells, I, at a rate

β. Infected cells produce virus at a rate p and die at a rate δ, while virions are cleared at a rate c. The above model is different from other models of virus dynamics due to its simplicity. This model can be used as a basis to understand infection parameters that are difficult (or impossible) to determine experimentally. One of the first applications of this simple model to experimental data was the analysis of in vivo HIV infection in 1996 [72]. A model similar to (3.1) was used to estimate the lifespan of infected cells and the rate of virion clearance. The model estimated that the production of virus by HIV-infected cells was substantially greater than previous estimates. That same year, a similar model was used to describe the dynamics of hepatitis B virus infection, providing estimates of viral clearance and production [61]. Subtle variations of this model have also been used to model hepatitis C [57] and influenza [1] infections.

3.1 Threshold of infection growth

When modelling viral infections, it is important to determine if an infection will spread throughout a cell population, or if the infection will be quickly extinguished. One way to visualize this is to consider a completely susceptible cell population infected with a small initial amount of virus. Susceptible cells will become infected by this initial amount of virus, thereby producing virions which subsequently go on to infect new cells. This continues until all cells become infected, or some equilibrium is reached e.g. if susceptible cells are produced at the same rate they are lost. However, in some cases the infection may not efficiently spread to nearby susceptible cells. For example, this could be due to the cells' lack of susceptibility to infection. Ideally, one would like to quantify under what circumstances this occurs. One means of determining if the infection spreads is with the use of a metric called the basic reproductive number, denoted R_0. In epidemiology, the basic reproductive number is defined as the mean number of secondary infections caused by a single infected individual in an otherwise susceptible population. The definition of the basic reproductive number is

similar for in-host infections; however, the number of secondary infections caused by a single infected cell, rather than a single infected individual, is used.

The basic reproductive number provides a simple threshold for determining if an infection will spread through a population. If $R_0 = 1$, then each infected cell infects exactly one other cell within it's lifespan. This ensures that the population remains constant, as the initially infected cell will be replaced by the newly infected cell only. If $R_0 > 1$, then the number of secondary cases is sufficient to replace the initial infected cell, and the number of infected cells will grow exponentially, as each newly infected cell will infect many other cells. However, if $R_0 < 1$, there are not enough secondary infections to replace the initially infected cell, and growth of the infection is suppressed.

In deterministic systems, the basic reproductive number can be found through a number of different methods, such as the survival function method and the next generation method, which are reviewed in detail in [35]. Many of these methods produce different values for the basic reproductive number; however, all of these methods interpret $R_0 = 1$ as a threshold of infection growth.

In ODE models of infectious disease, a linear stability analysis provides insight into the threshold behaviour of the basic reproductive number. Suppose we have a system of ODEs of the form

$$\dot{\mathbf{x}} = A\mathbf{x} \tag{3.2}$$

where $\mathbf{x} = (x_1, x_2..., x_n)$, A represents a matrix containing parameter values of the system and $\dot{\mathbf{x}}$ denotes the derivative of the vector $\mathbf{x}$ with respect to time. One can then find the fixed points of the system, $\mathbf{x}^*$, defined as

$$A\mathbf{x}^* = 0. \tag{3.3}$$

The system (3.2) is then linearized about the fixed points, producing a Jacobian matrix. The basic reproductive number is determined by finding the positive eigenvalue of the linearized

system; that is, when the system contains an unstable fixed point.

We can illustrate this concept by working through a simple example; let us consider the system given by equations (3.1). The uninfected equilibrium of the system can be given by the fixed point $(T^*, I^*, V^*) = (T_0,\, 0,\, 0)$, where T_0 is the initial number of susceptible cells. Linearizing system (3.1) about the fixed points gives

$$\begin{pmatrix} \dot{T} \\ \dot{I} \\ \dot{V} \end{pmatrix} = \begin{pmatrix} 0 & 0 & -\beta T_0 \\ 0 & -\delta & \beta T_0 \\ 0 & p & -c \end{pmatrix} \begin{pmatrix} T \\ I \\ V \end{pmatrix}.$$

Solving the eigenvalue problem

$$A\mathbf{x} = \lambda \mathbf{x}$$

leads to the characteristic equation

$$-\lambda \left[(\delta + \lambda)(c + \lambda) - p\beta T_0\right] = 0.$$

Solving this equation for the eigenvalue λ, we find that a positive eigenvalue (and therefore an unstable fixed point) exists if and only if

$$\frac{p\beta T_0}{\delta c} > 1,$$

given that the parameter values are all positive. We therefore define the threshold condition as

$$R_0 = \frac{p\beta T_0}{\delta c}, \tag{3.4}$$

where $R_0 > 1$ implies growth of the infection, and $R_0 < 1$ implies that growth of the infection will be suppressed. Thus, large values for parameters which add to the population of infected cells and virions (β and p, respectively) increase the chance that infection will spread, while large values for parameters which contribute to the removal of infected cells and virions from the system (δ and c, respectively), decrease the chance of infection spreading.

3.2 Mathematical models of influenza infection

Few attempts have been made to model within-host influenza infection dynamics mathematically. The first such model attempted to classify viral infection data using compartment models, consisting of seven separate compartments and five rate parameters [44]. While the model provided reasonable fits to experimental data, parameter values were not specifically related to within-host behaviour. In addition, the immune system was not taken into account in this model. However, the model provided evidence that complicated within-host infection data could be modeled using a simple deterministic approach.

Another mathematical model attempted to fully characterize the behaviour of within-host influenza infection by taking into account a substantial immune response [6]. The model consists of 13 variables, representing the virus, epithelial cells and various immune responses, and the behaviour is characterized by more than 60 parameters. Parameter values were estimated from experimental data, and an attempt was made to account for experimentally known infection dynamics, such as estimates of immune system activation, proliferation and decay rates at various times post-infection. However, the results of the model were not compared with experimental viral load or immune response data. Isolating the role of specific immune effects also proved difficult, due to the large number of parameters. More recently, a model consisting of 10 equations and 27 parameters, was developed, but the results were also not directly compared to experimental data due to the difficulty and cost in procuring such extensive viral and host immune response data [30].

The first mathematical model of influenza kinetics to take experimental data into account was proposed by Baccam et al. [1]. Data was taken from experimental infection of volunteers with the influenza A/Hong Kong/123/77 (H1N1) virus, a seasonal strain of the influenza virus which follows the typical course of an uncomplicated influenza infection. Nasal washes were collected daily and serially cultured in 10-fold dilutions to determine viral titers. The simple mathematical model used to describe the kinetics of infection is given by

$$\begin{aligned}
\frac{\mathrm{d}T}{\mathrm{d}t} &= -\beta TV \\
\frac{\mathrm{d}E}{\mathrm{d}t} &= \beta TV - kE \\
\frac{\mathrm{d}I}{\mathrm{d}t} &= kE - \delta I \\
\frac{\mathrm{d}V}{\mathrm{d}t} &= pI - cV \ ,
\end{aligned} \tag{3.5}$$

where target cells, T, are infected at a rate β by infectious virions, V, where the target cells become infected cells that are not yet producing virus, E, also called eclipse phase cells. Eclipse phase cells transition to productively infected cells, I, at a rate k. Productively infected cells die at a rate δ and produce virus at a rate p, while infectious virions, V, are cleared at a rate c. Infection is initiated by introducing an initial inoculation of virus V_0 to a population of susceptible target cells T_0. The model given by the system of equations (3.1) was also used to describe the infection; however, the authors determined that while it provided a reasonable fit to the data, the presence of an eclipse phase was more biologically realistic.

The initial population of target cells was determined using anatomical estimates, while the initial inoculation of virus V_0, as well as parameter values, were determined by fitting the model to the experimental data. As the effects of the immune system are not explicitly accounted for, the model is target-cell limited; that is, once the infection has spread, it stops only when the population of target cells has been entirely eliminated by the infection.

The model incorporating the eclipse-phase produced reasonable fits to the experimental data. The model suggested that cells are latently infected for around 6 h, before producing virus for approximately 5 h. The inclusion of the eclipse phase of infection does not change the equation for the basic reproductive number, which is given in Equation (3.4). The basic reproductive number in this case was estimated to be 22, suggesting that the infection spreads rapidly until all susceptible cells are infected. The model predicted that when the

viral titer reached its highest value, the proportion of dead cells varied from 37% to 66% between patients infected with the influenza A/Hong Kong/123/77 (H1N1) seasonal virus strain.

In this model, the regeneration of target cells was not considered. A term was included in the model for growth of target cells, but this additional term did not result in better fits to the experimental data. This could be due to the fact that fits to the experimental data found that virions are cleared 6–8 dpi, while regrowth of epithelial cells is not detected until near the end of the infection, around 5–7 dpi [91]. This suggests that the time scale for regrowth of epithelial cells is negligible compared to the length of infection.

A modification to the model which incorporated an interferon response was also studied in [1]; while it provided a better fit to the experimental data, the inclusion of additional parameters could not be justified given the limited amount of data available. However, given the limitations of the model, it proved to be adequate for characterizing key parameters of a viral infection, such as virus production rate and virion clearance rate, showing that a relatively simple mathematical model was able to sufficiently explain key features of influenza viral infections.

Recent models have used approaches similar to [1] in order to capture the dynamics of influenza infection using experimental data. For example, models have been developed to include the effect of antiviral drug treatment on influenza infection [5], as well as how antiviral drug resistance develops within-host, and how that resistance subsequently spreads in a population [31]. Models have also been developed to include the effect of the immune response to an influenza infection [32,46] by comparing models to experimental viral load data and immune response data. In order to provide fits to experimental data, the full immune response was not taken into account, and certain simplifications were made. However, in spite of these limitations, the models provided reasonable estimates of the experimental data.

3.3 Target cell heterogeneity in mathematical models

Although few mathematical models of within-host influenza infection have been attempted, other infectious diseases have been studied, providing a greater depth of knowledge regarding the virus dynamics of specific diseases. One example of this is the consideration of target cell heterogeneity, which has not yet been considered for within-host influenza infection, but has been considered to some extent for other infectious diseases.

One such example of target cell heterogeneity was investigated for patients infected with HIV-1 [71]. This model attempted to explain two different phases of decay of the virus during drug combination therapy by considering infection of susceptible T cells, as well as long-lived infected T cells and latently infected lymphocytes. The analysis found that these different cell types contribute to two different phases of viral decay. Another study looked at how lymphatic tissues, which may act as viral reservoirs, change the progression of HIV infection [2]. In both studies, different cell types were considered (such as macrophages and T-lymphocytes), as opposed to the same cell type with different infection characteristics (such as epithelial cells with different rates of infection).

Heterogeneous models have also been developed for hepatitis B virus by looking at infection of mature liver cells, or hepatocytes, and undifferentiated liver cells. It was assumed that viral replication within the two cell types would vary and that the two cell types may have different lifespans [65,66]. Although the model was able to describe some characteristics of clinical infection, the results were not compared against experimental data.

More recently, target cell heterogeneity has been considered in models of foot-and-mouth disease virus (FMDV) through epithelial cells [88]. This analysis set out to explain the existence of viral "reservoirs" in infected hosts, which can reignite infection weeks or months after infection was thought to have been cleared, by considering infection in different types of epithelial cells. However, this model is not directly applicable to influenza infections, which last for shorter periods of time than infection with the FMDV.

As discussed above, target cell heterogeneity is not a novel feature of virus dynamics models. However, the models described above assume infection of a wide variety of cell types, which share very few parameters. The presence of different compartments (such as additional types of virus or cells) with completely independent parameters also complicate the modelling process, as additional parameters must be justified through experimental data or through well known biological considerations.

3.4 Fitting models to experimental data

While mathematical modelling is an invaluable tool for understanding biological phenomena, including infectious disease dynamics, one must ensure that the model accurately describes experimental data. This is initially done by basing the model on sound biological reasoning, while ensuring realistic assumptions are made in the formulation of the model. To validate the model, it is important to compare its predictions to experimental data.

In order to quantitatively compare experimental results with mathematical predictions, least squares regression is commonly used. In this technique, the values of the free or unknown parameters in the mathematical model are estimated based on how well the ensuing curves produced by the model describe the experimental data. This comparison can be made using a quantity known as the sum of squared residuals, which is described using the formula

$$\text{SSR} = \sum_{i=1}^{n} (y_i - f(x_i))^2,$$

where $f(x_i)$ is the value predicted by the mathematical model and y_i is the experimental data point. In order to provide the best fit to the experimental data, the model parameters are adjusted such that the SSR is minimized.

Although the SSR specifies how closely a given model represents the experimental data, it does not specify if the given model provides a better fit to the data than other possible

model choices. In general, a model with a greater number of parameters will provide a better fit to experimental data, but the data may be insufficient to support the number of parameters. For example, a data set with 5 data points can only statistically support a model with fewer than 5 parameters. Thus, we would ideally like a model that minimizes the SSR, while also requiring the fewest number of parameters. One way to measure this is with a quantity known as Akaike's "an information criterion" or AIC. The AIC is given by

$$\mathrm{AIC} = n \ln\left(\frac{\mathrm{SSR}}{n}\right) + 2m,$$

where n is the number of data points, SSR is the sum of squared residual and m is the number of parameters [55].

The AIC represents a way of comparing how well different models fit the same set of data. Lower values of the AIC represent data fits that are better supported by the available data, as this represents a fit with a low SSR with a minimum number of parameters. Thus, the lower the AIC, the better the corresponding model is able to accurately represent the data.

Ideally, one would prefer $n \gg m$ to ensure an accurate fit of the model to the data, which the AIC accounts for by "penalizing" models with a small number of data points or a large number of parameters. However, when fitting data sets with a small number of data points (relative to the number of parameters), as is the case for experimental viral titer data, the corrected Akaike's "an information criterion" or $\mathrm{AIC_C}$ provides a more accurate method of comparing different models. The $\mathrm{AIC_C}$ is given by the equation

$$\mathrm{AIC_C} = n \ln\left(\frac{\mathrm{SSR}}{n}\right) + 2m + \frac{2m(m+1)}{n-m-1}.$$

The $\mathrm{AIC_C}$ is appropriate to use in all cases, as it generalizes to the AIC when $n \gg m$.

In the analysis that follows, experimental viral titer data was fit to the proposed model in order to determine the model parameter values. The fits were performed using an implementation of the Levenberg-Marquardt nonlinear regression method, an algorithm which

sets the optimal values of a model's parameters so as to minimize the SSR between the model and the data [76]. The AIC_C was used to compare the fits for models with different numbers of parameters. As mentioned above, the model with the lowest AIC_C is considered to better approximate the experimental data. Additional details of the fitting procedure are discussed in the ensuing chapter.

Chapter 4

Results [1] [2]

4.1 Introduction

The potential spread of a severe pandemic influenza is a worldwide cause for concern. In recent years, attention has focused on the avian-derived influenza A (H5N1) virus strain, which has the potential to evolve into a pandemic viral strain [62]. More recently, the swine-origin influenza A (H1N1) strain which is responsible for the current influenza pandemic has been a cause for concern as the northern hemisphere prepares for what could be a more serious outbreak in the coming influenza season given the strain's ability to cause severe illness and the added stress it will put on the health care system [13,23,25,42,59]. The reasons for the increased severity in pandemic-causing influenza strains are poorly understood and possible explanations include an excessive cytokine response [8, 9, 16, 41, 78], a poor immune response due to the strain's novelty [38, 77], and differences in target cell receptor affinity (cell tropism) between the two strains [51,53,69,81]. Recent work has focused on the binding

[1] A version of this chapter has been submitted for publication. M.J. Baron, H.M. Dobrovolny and C.A.A. Beauchemin, Influenza virus cell tropism in respiratory tract epithelial cells is sufficient to explain increased severity of highly virulent strains.

[2] The analysis in Section 4.3.4 of this chapter was performed by Dr. Hana M. Dobrovolny.

affinity of different strains of influenza virus for specific cell receptors within the respiratory tract [58,79,82,86] and it is believed that this difference in affinity between human and avian strains may in part be responsible for the difference in severity between the two strains, though the reasons for this are currently not well understood.

Two specific cell types are believed to play important roles in influenza virus infection: ciliated epithelial cells, and non-ciliated, mucus-producing cells. In epithelial cell cultures, non-ciliated, mucus producing cells predominantly express sialic acid α-2,6 galactose terminated saccharides (SAα2,6 Gal) on their surface, while ciliated cells express sialic acid α-2,3 galactose terminated saccharides (SAα2,3 Gal) receptors, as well as SAα2,6 Gal receptors, on their surface [39,43,82]. Within a human host, human-derived influenza A viruses (H1N1, H3N2) seem to preferentially bind to SAα2,6 Gal receptors, while avian-derived influenza A (H5N1) viruses appear to preferentially bind to SAα2,3 Gal cell receptors [51].

Recently, efforts have been made to model in-host influenza infection dynamics with a target cell limited model, using experimental data to validate the results [1, 5, 31], but the models have been limited to a single target cell population. Population heterogeneity has been accounted for in epidemiological models [19, 26, 36, 45], where individuals become infected through primary contact with an infected individual, and heterogeneity is introduced by varying the contact rates between subpopulations. Due to the absence of an intermediate infection agent (i.e., virions) in these models, their results are of limited applicability to in-host infections, where the infection progresses from infected cells to healthy cells via the production and dispersal of infectious virions. Target cell heterogeneity has also been considered for within-host models of HIV [2,71], hepatitis B [65,66] and hepatitis C [15] and has provided an explanation for multiple phases of infection [15, 71] or different courses of disease progression [2,65,66]. However, these models are fairly complex, containing multiple compartments [2,15] or assuming that target cell populations differ in most or all parameters [65, 66, 71].

Here, we propose a mathematical model consisting of two distinct cell populations which differ only in their susceptibility to infection by a given viral strain and their rate of viral production. This simple model allows us to study the effect of cell tropism on in-host disease progression and severity of influenza. By constraining one cell population to the specific parameter values defined in [1] for in-host human infection with influenza A (H1N1), we explore the dynamics of the model in the parameter space of the secondary population. We find that the parameter space contains a region of increased disease severity characterized by a larger viral titer peak and a long-lasting infection with high, sustained viral titer.

4.2 Materials and methods

4.2.1 Two target cell model of influenza infection

The proposed two target cell model, which consists of two cell populations both susceptible to influenza virus infection, is an extension of the differential equation model consisting of a single susceptible cell population and delayed viral production proposed in [1]. The model in [1] was fitted to match the dynamics of a primary influenza A/Hong Kong/123/77 (H1N1) infection in human volunteers, a seasonal strain of influenza which follows the typical course of an uncomplicated influenza infection. The model proposed in [1] was used to extract parameters for a typical human infection with a seasonal influenza strain, and these parameters are used as the basis for the proposed two target cell model. The proposed model consists of a population of default (subscript d) and secondary (subscript s) cells, namely

$$\begin{aligned}
\text{Target cells}: \quad & \frac{\mathrm{d}T_d}{\mathrm{d}t} = -\beta T_d V && \frac{\mathrm{d}T_s}{\mathrm{d}t} = -r_\beta \beta T_s V \\
\text{Eclipse cells}: \quad & \frac{\mathrm{d}E_d}{\mathrm{d}t} = \beta T_d V - kE_d && \frac{\mathrm{d}E_s}{\mathrm{d}t} = r_\beta \beta T_s V - kE_s \\
\text{Infected cells}: \quad & \frac{\mathrm{d}I_d}{\mathrm{d}t} = kE_d - \delta I_d && \frac{\mathrm{d}I_s}{\mathrm{d}t} = kE_s - \delta I_s \\
\text{Virus}: \quad & \frac{\mathrm{d}V}{\mathrm{d}t} = pI_d + r_p p I_s - cV \ .
\end{aligned} \tag{4.1}$$

Infection proceeds as target cells T are infected by virus V at a rate β (or $r_\beta\beta$). The newly infected cells E first enter a latent infection stage, called the eclipse phase, and turn into productively infected cells I at a rate k. Productively infected cells produce virus at a rate p (or $r_p p$) which is cleared at a rate c by the immune system or through loss of infectivity. The remaining virus then goes on to infect new target cells, and the infection progresses.

Differences between the two cell populations are controlled by three key parameters: r_β, r_p, and r_T. These parameters represent the ratio of the susceptibility to infection, r_β, and viral production rate, r_p, of the secondary cell type to that of the default cell type, and the fraction of cells of the secondary type in the initial target cell population, r_T. For example, setting $(r_T, r_\beta, r_p) = (0.2, 10^{-3}, 10^2)$ corresponds to a cell population where 20% of cells are of the secondary type and are 1,000-fold less susceptible to infection compared to cells of the default type, but once infected these secondary cells will produce 100-fold more virus than cells of the default type.

While r_β and r_p are scaling factors for parameters β and p in the secondary cells, respectively, r_T does not appear explicitly in the model as it is set through the initial conditions for target cells such that

$$\text{Initial target cells :} \qquad T_{d,0} = (1 - r_T)T_0 \qquad T_{s,0} = r_T T_0 \ ,$$

where $0 \leq r_T \leq 1$.

The total number of initial target cells is set to $T_0 = 4 \times 10^8$ cells, which is in line with anatomical estimates for the human upper respiratory tract [1]. Infection is initiated by an initial inoculation of virus V_0. Default parameter values and initial conditions for (4.1) were taken from [1] and are listed in Table 4.1. Numerical solutions of model (4.1) were obtained using the `lsode` function in Octave 3.0.1 [22], which uses an implementation of a backward differentiation formula (Gear's method) if the equations are stiff; otherwise, Adam's (predictor-corrector) method is used [37].

Table 4.1 Default initial conditions and parameter values of model (4.1).

Symbol	Values taken from [1]
T_0	4×10^8 cells
$E_{s,0} = E_{d,0} = I_{d,0} = I_{s,0}$	0
V_0	7.5×10^{-2} TCID_{50}/mL
β	3.2×10^{-5} $(\text{TCID}_{50}/\text{mL})^{-1} \times \text{d}^{-1}$
p	4.6×10^{-2} $\text{TCID}_{50}/\text{mL} \times \text{d}^{-1}$
k	4.0 d^{-1}
δ	5.2 d^{-1}
c	5.2 d^{-1}

4.3 Results

4.3.1 Mapping the parameter space

Since differences in cell receptor specificity between influenza A strains of human and avian origin, and changes in viral production for different cell types have not been quantified [51, 52, 92], we consider a wide range of parameter values for the secondary cell population. The susceptibility to infection of target cells of the secondary type, r_β, and their rate of viral production once infected, r_p, are independently varied from 1,000-fold less (10^{-3}) to 1,000-fold more (10^3) than that of the default cell type.

Figure 4.1 illustrates how the time post-infection at which viral titer peaks depends on the ratios of susceptibility to infection (r_β) and viral production rate (r_p) of the secondary cell type to the default cell type. Here we present only the case where default and secondary target cells are present in equal numbers ($r_T = 0.5$). Varying the fraction of target cells of the secondary type results in similar behaviour, except in the case of a nearly homogeneous

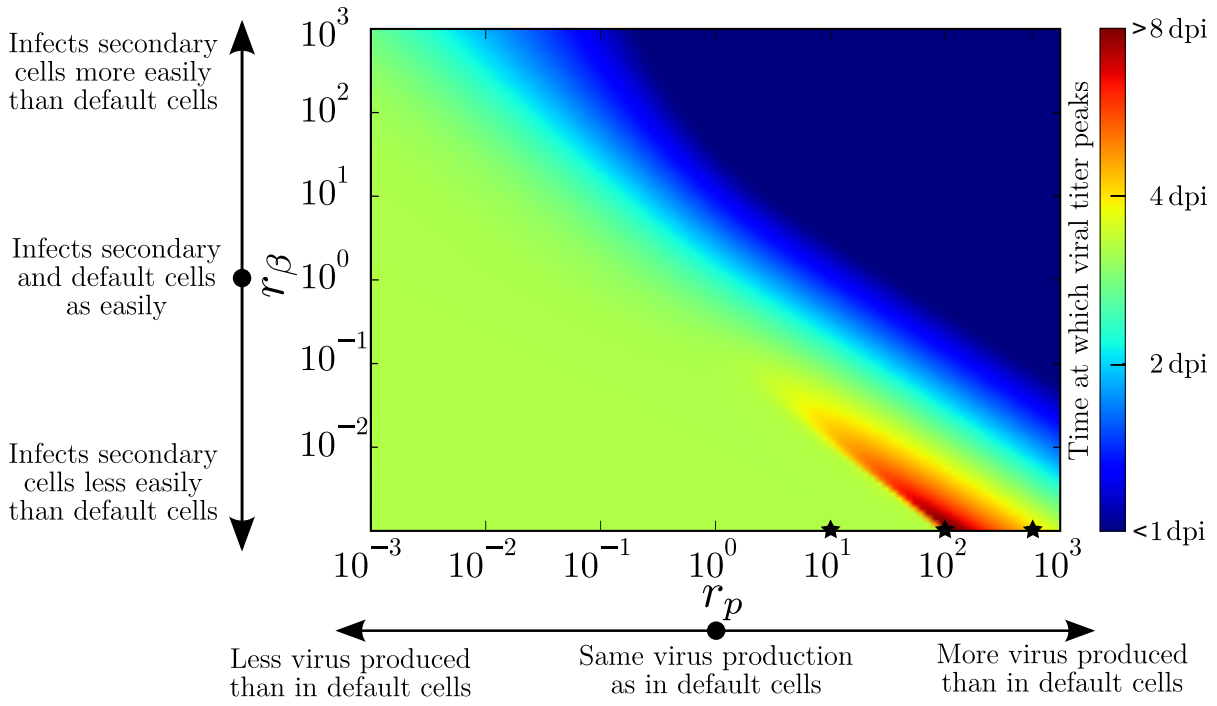

Figure 4.1 Time of viral titer peak for different properties of the secondary cell type. The effect of varying the secondary cells' susceptibility to infection (r_β) and their rate of viral production (r_p) relative to the default cell type is illustrated for a population of cells with an equal abundance of default and secondary cells ($r_T = 0.50$). All other parameter values are given in Table 4.1. Time of viral titer peak is given in days post-infection (see legend to the right of graph). The three stars indicate the specific parameter values for the plots in Figure 4.2.

secondary cell population ($r_T > 0.955$).

When $r_\beta = r_p = 10^0 = 1$, the two target cell model reduces to the single target cell model and the viral titer curve reaches a peak value around 3 days post-infection (dpi), as was found in [1]. Not surprisingly, increasing the secondary cells' susceptibility to infection (r_β) or their rate of viral production (r_p) relative to the default cell type causes the infection to peak earlier. This is because with a large r_β, cells of the secondary type are infected more easily and therefore consumed more rapidly by the infection leading to a shorter-lasting infection. Analogously, with a large r_p, secondary cells release larger amounts of virus once infected, which in turn leads to a more rapid consumption of all cell types by the infection.

This translates to a shorter-lasting infection as one moves upwards or rightwards on the graph in Figure 4.1, with the shortest-lasting infections found in the top right corner of the graph.

In general, over the parameter space explored, the viral titer peaks between 1 dpi and 4 dpi, with the exception of an unexpected pocket in the parameter space at the bottom-right of our graph in the region where cells of the secondary type produce around 100-fold more virus than cells of the default type ($r_p = 10^2$), but are 1,000-fold harder to infect ($r_\beta = 10^{-3}$). In the vicinity of this pocket, the time of viral peak varies rapidly from 2 dpi to more than 8 dpi, becoming increasingly sensitive to the secondary cells' susceptibility to infection and their viral production rate. Within this parameter region, secondary cells are not easily infected, due to their low susceptibility to infection (small r_β), and as such these cells are consumed very slowly by the infection. On the other hand, their high rate of viral production (large r_p) means that once infected, even in very small numbers, these cells produce large quantities of virus. As a result, the viral titer is sustained at high levels long after the onset of infection, and peaks substantially later than in other regions of the parameter space.

This is well illustrated in Figure 4.2 where the kinetics of the infection are shown for three different viral production rates of the secondary cell population for the case where these cells are 1,000-fold harder to infect than cells of the default type. When secondary cells produce only 10-fold more virus than cells of the default type, the infection is mostly limited to the default cell population as the amount of virus produced is not sufficient for the infection to spread to the secondary cell population. Increasing the production rate to 100-fold more than cells of the default type results in a sufficient amount of virus being produced to sustain a slow growing infection within the secondary cell population, leading to long-lasting, high-levels of viral titer. Finally, increasing the viral production rate to 1,000-fold more than the default cell type allows the infection to successfully infect and decimate both cell populations rapidly. From these results, we see that there appears to be a relationship

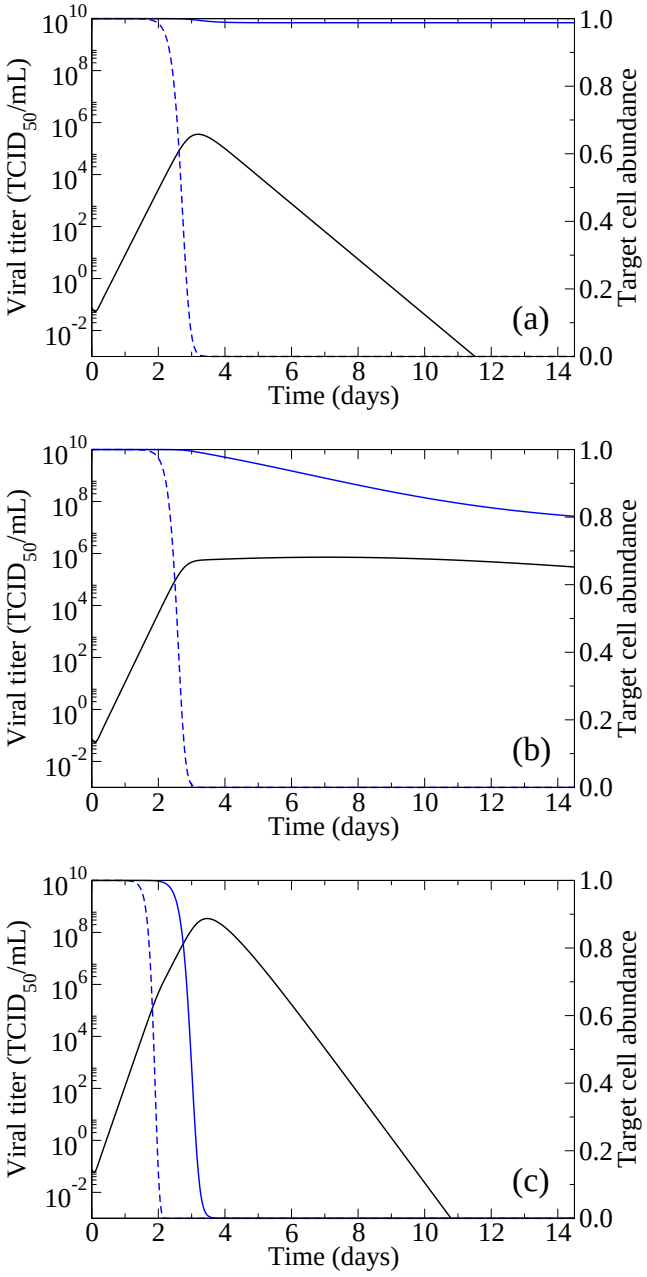

Figure 4.2 Effect of increasing secondary cells' viral production rate at low infection rate. The amount of viral titer (black), and the relative abundance of target cells of the default (blue, dashed) and secondary (blue, solid) type over the course of an in-host influenza infection are shown for different viral production rates by secondary cells, r_p, of (a) 10-, (b) 100-, and (c) 1,000-fold higher than that for cells of the default type. The fraction of target cells of the secondary type, r_T, is 0.5, and the secondary target cells' susceptibility to infection is r_β = 1,000-fold less than for cells of the default type. All other parameters are as in Table 4.1.

between the secondary cells' susceptibility to infection and their viral production rate which leads to a severe and sustained infection.

4.3.2 Conditions for infection

In order to better understand the relationship that needs to exist between the secondary cell population's susceptibility to infection and viral production rate to give rise to a severe, long-lasting infection, it is useful to consider a linear stability analysis of the two target cell model. For all parameter values, the equations have a line of fixed points, corresponding to a stable, uninfected cell population persisting in the absence of infection, namely $(T^*, E^*, I^*, V^*) = (T_{\text{eq}}, 0, 0, 0)$, where $T_{\text{eq}} = T_{\text{eq},d} + T_{\text{eq},s}$. Within both default and secondary cell types, the fixed point (or equilibrium value) is less than or equal to the initial cell population, i.e., $T_{\text{eq},d} \leq T_{0,d}$ and $T_{\text{eq},s} \leq T_{0,s}$. Therefore, the stability of a fixed point is guaranteed by the condition $R_s + R_d < 1$, where

$$R_d = \frac{\beta p T_{0,d}}{\delta c} \qquad\qquad R_s = \frac{(r_\beta \beta)(r_p p) T_{0,s}}{\delta c} \ ,$$

$T_{0,d} = (1 - r_T)T_0$ and $T_{0,s} = r_T T_0$. Thus, when $R_s + R_d < 1$, an initial quantity of virus does not lead to a substantial infection of the cell population, and growth of the virus is suppressed. For a single target cell population, i.e., $r_T = 0$ or $r_T = 1$, the stability conditions are $R_d < 1$ or $R_s < 1$, respectively.

The three quantities, R_s, R_d and their sum, are analogous to the basic reproductive number R_0, a frequently used quantity in epidemiology and virus dynamics, which is defined as the average number of second-generation infections produced by a single infected cell within a uniform population of completely susceptible cells [60,85]. Although this description of R_d and R_s may be valid in the case of a homogeneous cell population, the interpretation for a heterogeneous population is less straightforward.

For the parameter values presented in Table 4.1, the quantity R_d is always greater than one when $r_T < 0.955$, resulting in growth of the viral titer. This results from the choice

of default parameter values, which were taken from an infection where $R_0 > 1$. When $r_T > 0.955$, regions arise within the parameter space where $R_s + R_d < 1$; that is, the initial viral titer fails to lead to an infection. We also see a region where the individual quantities R_d and R_s are both less than one, but the sum of these quantities is greater than one. This implies that the infection grows slowly, and although not explicitly accounted for in our model, the host immune response would likely intervene before the viral titer reached symptomatic levels. These cases are illustrated in Figure 4.3.

In order to narrow our focus to biologically relevant regions of the parameter space, we will restrict our analysis to the case where $r_T < 0.955$. The quantity $R_s = 1$ will be seen to form a boundary in the parameter space which establishes a region leading to high viral loads which are sustained for long periods of time.

4.3.3 Measures of disease severity

Beyond mapping the infection kinetics through the parameter space, it is important to understand the implication of a given viral titer curve on the severity of infection for a patient. To this end, we introduce three measures of viral infection severity: time of viral load peak, duration of symptomatic infection and total amount of virus. Each measure has its advantages and limitations, but together they provide a better understanding of the infection dynamics in terms of how it may be experienced by a patient.

In order to focus on the specific parameter region which results in severe, long-lasting infections characterized by high-level, sustained viral loads, we restrict our analysis to the region of the parameter space bounded by r_β, the relative susceptibility of secondary cells to infection, from 10^{-6} to 10^0, and r_p, the relative viral production rate by secondary cells, from 10^0 to 10^6.

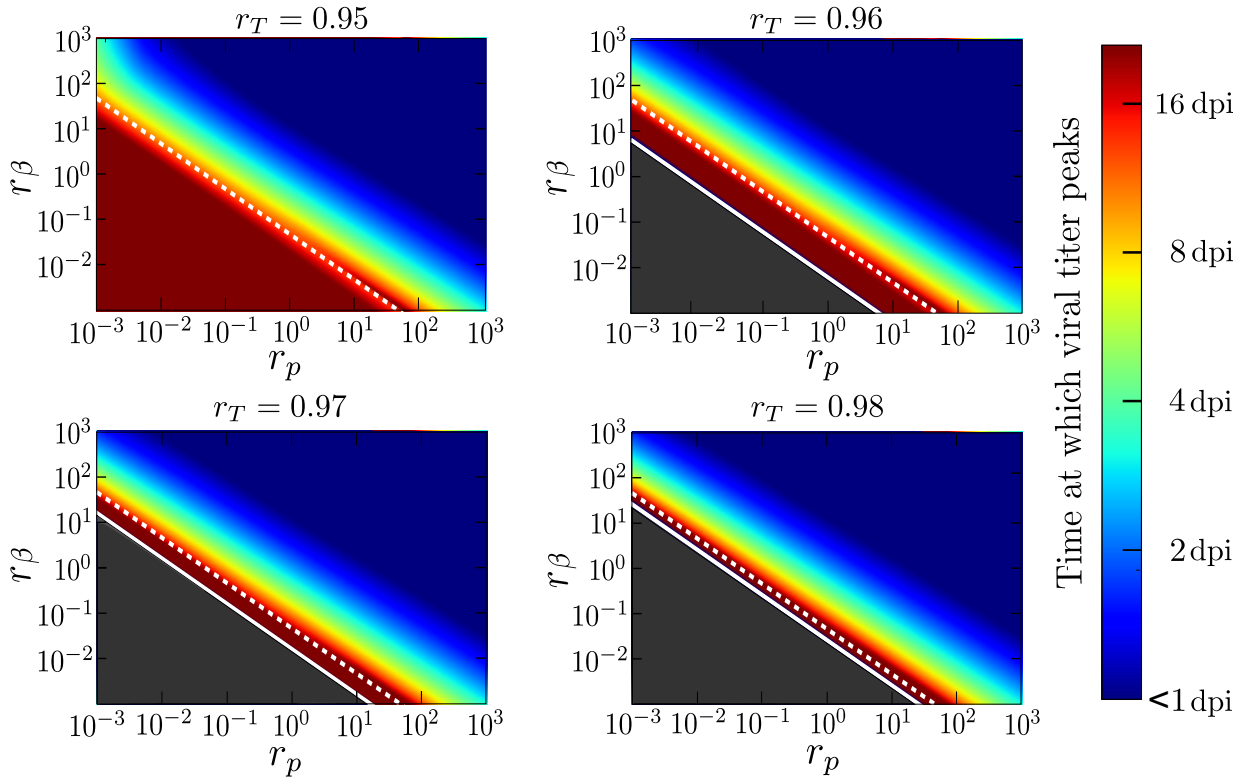

Figure 4.3 Time of viral load peak when the cell population is mostly composed of secondary cells. Different graphs represent different proportion of secondary target cells, r_T, ranging from 0.95–0.98. Each graph explores the effect of varying the secondary cells' susceptibility to infection (r_β) and their rate of viral production (r_p) relative to the default cell type. All other parameters are held fixed at the values presented in Table 4.1. The stability conditions $R_s = 1$ (dashed white line), and $R_s + R_d = 1$ (solid white line) are also indicated. Grey regions indicate cases where the infection fails to spread to either cell population. Time of viral titer peak is given in days post-infection (see legend on right side of graphs).

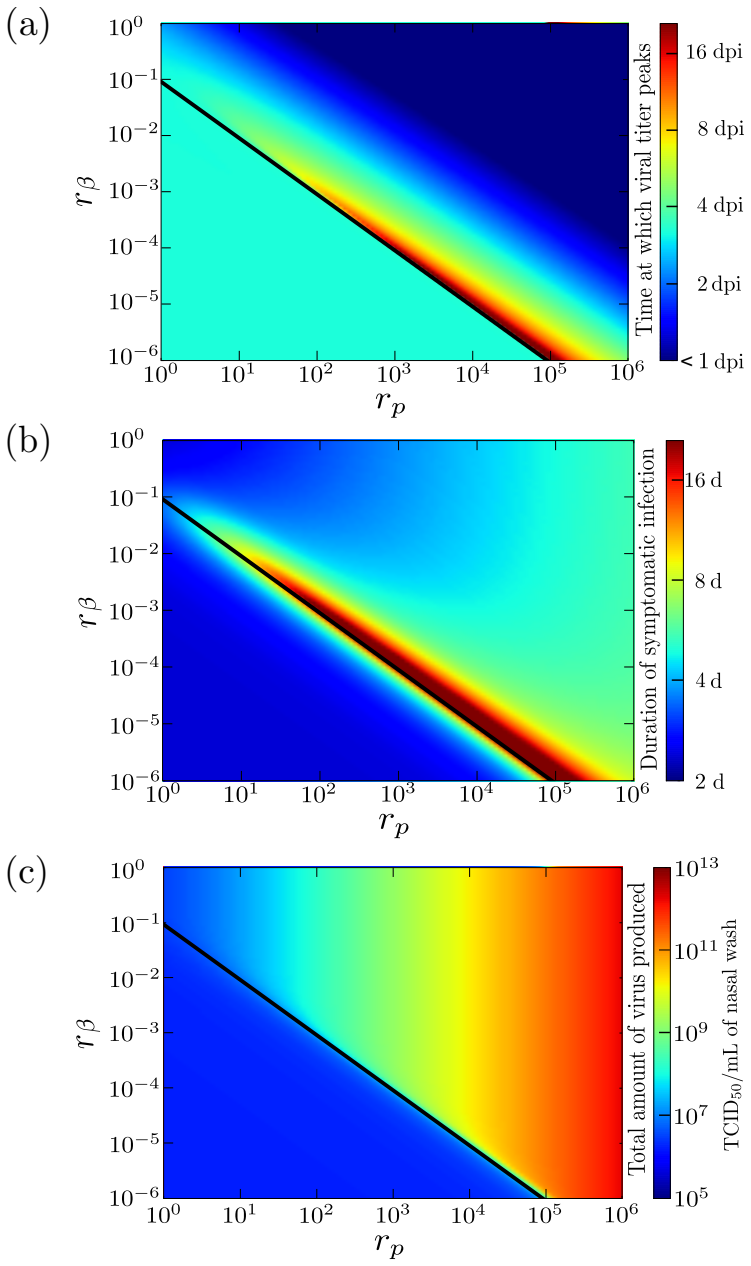

Figure 4.4 Measures of disease severity for varying properties of the secondary cell population. The effect of varying the secondary cell's susceptibility to infection (r_β) and their rate of virus production (r_p) compared to that for cells of the default type on different measures of disease severity: (a) time of viral titer peak, (b) duration of symptomatic infection and (c) total amount of virus produced. Note that the value of the disease severity measures in the top left corner of each graph ($r_\beta, r_p = 1,1$) corresponds to the single target cell model. All other parameters are set as specified in Table 4.1, with $r_T = 0.5$. The stability condition $R_s = 1$ is also indicated (black line).

Time of viral titer peak

A useful measure of disease severity is the time at which the viral load reaches a maximum value. This is an important measure because, as seen in [1], when treatment with a neuraminidase inhibitor such as oseltamivir is applied after viral titer peak, it has little effect on disease severity and duration. Thus, the time of viral titer peak provides an estimate of the time window available for effective treatment. In general, an early viral titer peak means that both external treatment or host immunity has little opportunity to act to reduce disease morbidity. The dependence of the time of viral titer peak on the secondary cells' infection characteristics are shown in Figure 4.4(a).

As the secondary cells' susceptibility to infection (r_β) and their viral productivity (r_p) decrease, the viral titer peaks progressively later, going from 1 dpi to as late as 16 dpi. This occurs when $R_s > 1$, i.e., when the infection is sustained within the secondary cell population. In the region where $R_s \sim 1$, the late peak of viral titer is due to the inability of secondary cells to become easily infected, combined with their ability to produce vast quantities of virus once infected. This late viral titer peak means that even relatively late treatment would have a noticeable, beneficial effect in reducing disease morbidity and perhaps avoiding mortality in such infections.

Symptomatic infection duration

Though our model predicts that viral titer can peak significantly later for certain parameter regimes, this does not necessarily imply a more severe infection. For example, it is important to distinguish between a small, slow growing infection, and one which grows rapidly and is maintained over a long period of time, with a late viral titer peak. While the former would likely be cleared effectively by an immune response before it has the chance to fully develop, the latter might already be too severe by the time the immune response gets underway, resulting in a severe infection rendered more morbid by the extensive immune response

triggered by the high and long-lasting viral titer. Thus, we establish another measure of infection severity, which we define as the length of the symptomatic infection. The dynamical markers for disease severity are not well known, but based on patient symptom scores, the onset of symptoms in a human-derived influenza infection appears to take place sometime between 1–2 dpi, and to dissipate around 5–6 dpi [24, 33]. On the viral titer curves for human-derived strain infection, these two time points correspond to places where the viral titer curve crosses 10^4 TCID_{50}/mL (see Figure 4.2(a)). Thus, we set this as the viral titer threshold for symptomatic infection. Following this convention, we define the duration of the symptomatic infection to be the length of time for which the viral titer remains above the symptomatic threshold. This is shown in Figure 4.4(b).

We find that the region corresponding to a late peak of the viral load in Figure 4.4(a) also corresponds to a viral load sustained above the symptomatic threshold long after the onset of infection. The viral titer surpasses the symptomatic threshold approximately 2 dpi, as we can see in Figure 4.2(b). We can therefore rule out the possibility that the late peak of the viral titer is a consequence of slow and steady growth of the viral titer. Rather, the late peak is the result of sustained viral titer at high levels. This behaviour can be explained by considering the infection of the two populations separately. After the default cell population is completely consumed by the infection, approximately 3 dpi, an essentially homogeneous population of secondary cells remains. The quantity R_s is then analogous to the basic reproductive number for the secondary cell population. Thus, when R_s is slightly greater than one, growth of viral titer occurs slowly, and the viral titer is sustained at the high levels produced during infection of the default cell population, as illustrated in Figure 4.2(b). This also has implications for treatment strategies. While a long lasting treatment regimen usually makes little sense for treating seasonal influenza infections, it would be beneficial if not necessary for controlling a longer-lasting infection characterized by sustained viral production.

Total virus produced

In assessing infection severity, it is also helpful to consider the total amount of virus produced over the course of the infection. Severe influenza viral infections are characterized by high viral loads [17], which does not necessarily follow from a delayed peak of the viral titer or a long symptomatic infection. The total amount of virus produced during the course of infection was determined using

$$V_{\text{total}} = \int_0^\infty (pI_d + r_p pI_s)\, \mathrm{d}t.$$

The results within the parameter space are shown in Figure 4.4(c). When $R_s < 1$, the total amount of virus produced is independent of r_β and r_p as the viral titer does not grow to sufficient levels to establish an infection within the secondary cell population. When $R_s > 1$, there are sufficiently large rates of viral production and target cell infectivity for the infection to spread within the secondary cell population. Figure 4.4(c) illustrates that when $R_s > 1$, the amount of virus produced is predominantly dependent on the scaling factor for the rate of viral production, r_p. When r_p is large, a significant amount of viral titer is produced and a large number of cells from both populations are consumed, regardless of the secondary cells' susceptibility to infection. However, as r_p decreases, the quantity R_s approaches one, and the presence of long-lasting infection becomes increasingly sensitive to variations of both r_p and r_β.

This feature is particularly interesting when framed within the context of anti-influenza drug treatment. For infection characterized by $R_s > 1$, depending on the value of r_p and r_β, i.e. where you are in the parameter space, it is sometimes preferable to treat with an antiviral targeting the secondary cells' susceptibility to infection, r_β, such as an adamantane so as to move downwards in the parameter space to most easily reach $R_s < 1$. In other cases, it would be much more beneficial for an equivalent drug efficacy to treat with an antiviral targeting the secondary cells' viral production rate, r_p, such as a neuraminidase inhibitor so as to move leftwards in the parameter space to most easily reach $R_s < 1$.

4.3.4 Fitting the model to data

We have seen that the two target cell model is capable of producing sustained viral titers. To determine whether these sustained viral titers actually model real influenza infections, we fit the two target cell model to measurements of influenza infections in mice [73] and humans [16]. In the first data set, BALB/c mice were infected intranasally with 10^2 pfu of A/Texas/36/91 (H1N1), A/1918 (H1N1), A/Thailand/SP/83/2004 (H5N1), or A/Thailand/16/2004 (H5N1) influenza virus. Lungs from 3 mice were harvested and homogenized at 1, 3, 4, 5, and 7 dpi. Virus titers were determined by plaque assay in MDCK cells. Although two strains are avian and two strains are human, all four produced infections with sustained viral titers. Although this may seem unusual given the predominant belief that avian-strain influenza dynamics are different from human-strain influenza dynamics, similar results have also been seen in influenza infections of ferrets [49, 84], mice [27, 47], and swine [48], as well as MDCK cell cultures [74, 94] and human tissue cell cultures [53, 73]. The second data set consists of pharyngeal and nasal swabs collected from 18 patients infected with avian (H5N1) influenza and 6 patients infected with human influenza (either H1N1 or H3N2) upon admission to hospital. This data set shows a clear dynamical difference between human-strain and avian-strain influenza, with avian-strain influenza infection peaking later and lasting longer than the human-strain infection.

Since the two target cell model has more parameters than there are data points, we fixed the parameters $1/k = 1/4$ d, $c = 5.2$ d^{-1}, and $1/\delta = 1/2$ d to values determined in [1] for a human infection with influenza A/HK/123/77 (H1N1). Although these parameters may be different for infection with different influenza strains, we believe that differences in cell tropism (β, r_β) and viral productivity (p, r_p) are most critical to differences in dynamics between influenza strains. We also fix $r_T = 0.3$ based on studies of the mouse lung which indicate that the mouse tracheal epithelium consists of approximately 30% ciliated cells [64] and on studies of human lung physiology indicating that the epithelium of the upper airway

(up to the fifth generation) comprises 50–85% non-ciliated cells [14] (this tacitly assumes that the ciliated cells are the default or preferred cells). Setting an exact value for r_T is not essential since a change in r_T can be corrected by appropriate re-scaling of p and r_p. That is, if $r'_T = \alpha r_T$ then we have

$$\begin{aligned} \text{Target cells :} \qquad & T'_d = \alpha T_d \qquad & T'_s = (1-\alpha) T_s \\ \text{Production rate :} \qquad & p' = \frac{p}{\alpha} \qquad & r'_p = \frac{\alpha}{(1-\alpha)} r_p. \end{aligned} \tag{4.2}$$

All other parameters were determined by fitting $\log_{10}(V)$ predicted by numerically solving the model to $\log_{10}$ of the experimental viral titer. The fits were performed using the Octave 3.0.1 [22] `leasqr` function, which is an implementation of the Levenberg-Marquardt nonlinear regression method [76].

For comparison, we also fit the data using the single target cell eclipse model [1]. To quantify the quality of each fit, we computed the sum of squared residuals (SSR) between the experimental viral titer and the models' results. In order to compare models with different numbers of parameters, we also computed small-sample size (second order) Akaike's "an information criterion" (AIC_C). The model with the lowest AIC_C is considered to be the better model given the experimental data it is approximating.

In Figure 4.5, which shows our model fits to influenza infections in mice, it is visually apparent that the two target cell model captures the dynamics of the infections much better than the single target cell model. This is corroborated by the lower SSR of the two target cell model, 0.41 versus 13 for the single target cell model. A lower SSR for the two target cell model is not unexpected since it has many more parameters than the single target cell model. The AIC_C, which corrects for differing numbers of parameters, however, indicates that we are over-fitting the limited data when using the two target cell model. In the accompanying table, we see that all four strains prefer ciliated cells ($R_d > R_s$). Ciliated cells are thought to be the preferred cell type for avian-strain influenza, but human-strain influenza is thought to prefer non-ciliated cells [51]. It is interesting to note that our model suggests that for all

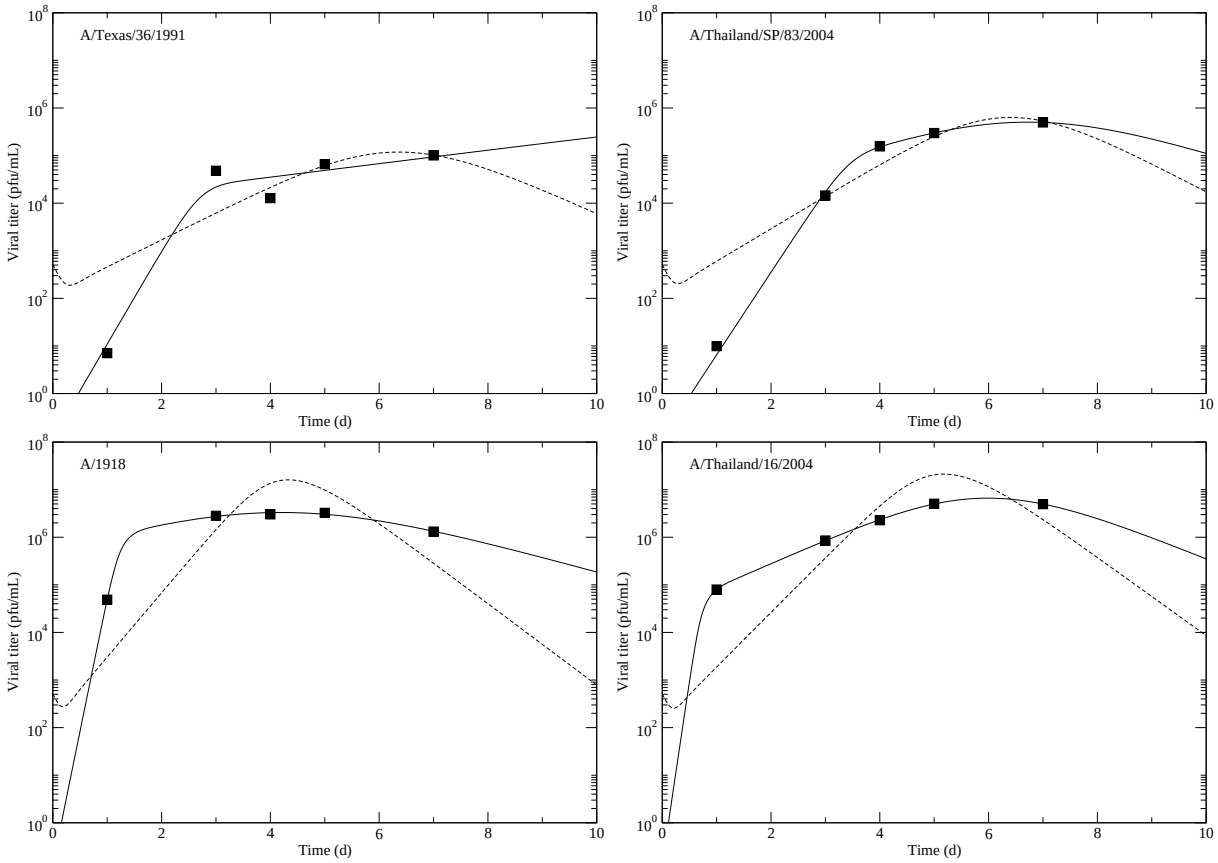

Figure 4.5 Model parameter fits to experimental influenza virus infections in mice. Results of parameter fits of the two target cell (solid line) and single target cell (dashed line) models to viral titer of mice infected with different influenza strains (black squares). We fixed the duration of the eclipse phase ($1/k = 1/4$ d), the lifespan of infected cells ($1/\delta = 1/2$ d), and the clearance rate ($c = 5.2\ \mathrm{d}^{-1}$). The percentage of default (ciliated) cells is fixed to 30%. Units of viral titer, $[V]$, are pfu/mL. Data is taken from [73].

Table 4.2 Model parameter fits for experimental influenza infection in mice.

Strain	V_0 ([V])	β $(([V]\cdot d)^{-1})$	p $([V]\cdot d^{-1})$	r_β	r_p	R_d	R_s	SSR	AIC_C
Two Target Cell Model									
A/TX/36/91	0.44	5.0×10^{-4}	8.1×10^{5}	3.2×10^{-5}	1.5×10^{3}	12	1.3	0.41	640
A/Thai/SP/83/04	idem	8.2×10^{-5}	3.7×10^{6}	8.9×10^{-3}	11	8.7	1.9		
A/1918	idem	8.0×10^{-5}	4.7×10^{7}	1.0×10^{-3}	6.4	110	1.6		
A/Thai/16/04	idem	2.6×10^{-3}	3.1×10^{3}	3.6×10^{-5}	1.3×10^{2}	230	2.5		
Single Target Cell Model									
A/TX/36/91	510	6.6×10^{-6}	4.3×10^{6}	–	–	2.7	–	13	37
A/Thai/SP/83/04	idem	1.8×10^{-6}	1.9×10^{7}	–	–	3.3	–		
A/1918	idem	2.7×10^{-7}	2.8×10^{8}	–	–	7.3	–		
A/Thai/16/04	idem	1.5×10^{-7}	4.1×10^{8}	–	–	5.9	–		

four influenza strains the secondary (non-ciliated) cell population is much harder to infect ($r_\beta \approx 10^{-3}$–10^{-5}), but produces more virus when it is infected ($r_p \approx 10$–10^3) and that all four strains have a large value for R_d and a value of R_s slightly larger than 1, indicating that both cell types are involved in the infection and that the infection grows slowly in the secondary (non-ciliated) cells. This corresponds to the pocket of sustained viral titer seen in Figure 4.1.

Figure 4.6 shows several fits for human- and avian-strain influenza infections in humans. The solid line uses the two target cell model for the avian-strain infection and the single target cell model for the human-strain infection. The dashed line uses the single target cell model for both strains and the dotted line uses the two target cell model for both strains. The SSR and AIC_C are lowest when the two target cell model is used to fit the avian-strain infection and the single target cell model is used to fit the human-strain infection. This suggests that while human-strain influenza infections are adequately described by a model that considers only a single target cell population, avian-strain influenza infections require another element, such as a secondary cell population, to explain the delayed viral titer peak and sustained viral titer. It is interesting to note that when using the two target cell model,

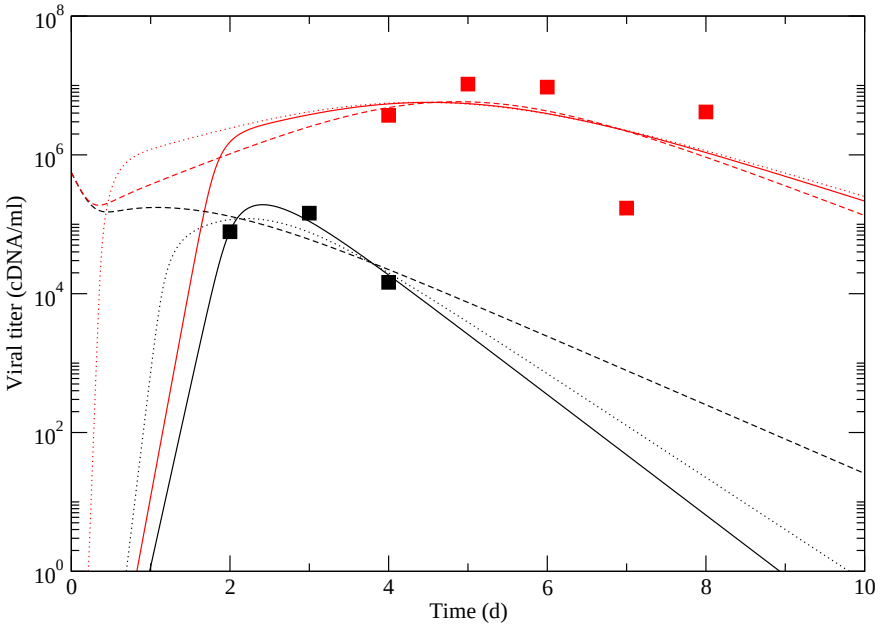

Figure 4.6 Model parameter fits of human and avian influenza virus infections in humans. Results of parameter fits of natural human infections with either a human (black squares) or avian (red squares) influenza strain. The data was fit using the single target cell (dashed) or the two target cell (dotted) model for both strains or the single cell model for the human strain and the two cell model for the avian strain (solid). We fixed the duration of the eclipse phase ($1/k = 1/4$ d), the lifespan of infected cells ($1/\delta = 1/2$ d), and the clearance rate ($c = 5.2$ d^{-1}). The percentage of ciliated cells is fixed to 30%. Units of viral titer, $[V]$, are cDNA/mL. Data is taken from [16].

Table 4.3 Model parameter fits for influenza infection in humans.

Strain	V_0 ([V])	β (([V]$\cdot$d)$^{-1}$)	p ([V]$\cdot$d^{-1})	r_β	r_p	R_d	R_s	SSR	AIC$_C$
Solid Line									
Avian	2.6×10^{-5}	6.2×10^{-5}	7.5×10^{7}	1.0×10^{-3}	5.5	130	1.8	1.9	-140
Human	idem	4.0×10^{-4}	3.4×10^{6}	–	–	91	–		
Dashed Line									
Avian	5.6×10^{5}	9.1×10^{-8}	3.8×10^{8}	–	–	2.3	–	2.1	85
Human	idem	4.0×10^{-6}	7.0×10^{6}	–	–	1.9	–		
Dotted Line									
Avian	8.3×10^{-7}	9.1×10^{-3}	3.5×10^{7}	6.3×10^{-6}	14	9200	1.9	2.0	-64
Human	idem	1.7×10^{-5}	5.3×10^{6}	2.9×10^{2}	0.22	2.6	400		

our fits predict that the ciliated cells are more easily infected with avian-strain influenza ($r_\beta < 1$) and the nonciliated cells are more easily infected with human-strain influenza ($r_\beta > 1$), as is seen in experiments [53].

4.4 Discussion

It has been suggested that differences in disease severity between human- and avian-derived influenza virus infections may in part be due to differences in target cell tropism between the two viral subtypes [39, 51]. In order to determine how cell tropism affects the dynamics of an influenza virus infection, we developed a mathematical model consisting of two different target cell populations: a default and a secondary population. The secondary cell population differs from the default population only in its susceptibility to infection and rate of viral production.

We found that within a certain area of the parameter space, the viral load in the two target cell infection model quickly rises to high levels and high viral production is maintained over extended periods of time. This type of viral load profile cannot be obtained with the standard single target cell model [1,5,80], but may be characteristic of infections with avian-derived influenza strains [16, 78]. The two target cell model displays this behaviour when the cells of the secondary population are more difficult to infect than those of the default population, but produce larger amounts of virus once successfully infected. The infection proceeds when the default cell population falls prey to the infection and is consumed rapidly ($\sim$ 2 d). This in turn increases the viral load to levels sufficient to initiate infection of the more refractory secondary cell population. Once infection is established within the secondary population, the high viral load produced by these cells is sufficient to sustain their slow but steady consumption by the virus, resulting in a long and severe infection. Fits of the two target cell model to viral titers of influenza infections in mice and humans support this scenario as a possible explanation of sustained viral titers.

It has been noted that ciliated cells are likely the primary target cells for avian-derived influenza virus strains [51], while non-ciliated cells are also susceptible to infection by avian viruses but to a smaller extent [53]. Within the framework of our two target cell model the ciliated cells would be the default cell population while the non-ciliated cells would represent the secondary population. Once infected, the non-ciliated (secondary) cells would have to produce much larger amounts of virus than their ciliated counterparts in order to yield the high sustained viral load which have been seen in human infections with avian-derived strains [16]. This is plausible given that non-ciliated cells, due to their mucus production activity, likely have a higher viral throughput than ciliated cells. While this is exactly the result we find with our model fits to avian-strain influenza infections in humans and mice (Figures 4.5 and 4.6), we also find that human-strain influenza infections in mice also seem to prefer ciliated cells. Our finding, coupled with other experimental data suggesting sustained viral titers can be produced by human-strain infections [27, 47–49, 53, 73, 74, 84, 94], leads to uncertainty over the nature of the interaction of different viral strains with different cell types. If these two cell types' specific susceptibility to infection and viral productivity were experimentally quantified for infections with human- and avian-derived strains, it would be possible to determine exactly the extent of the effect of cell tropism on disease severity.

If human infections with avian-derived influenza strains do in fact lead to high viral loads sustained over several days as some data suggests [16, 78], it is important to consider the implications of this viral titer profile for antiviral treatment strategies. A high viral load sustained over several days results from either the sustained viral production of an ongoing infection or from the lingering of already secreted viral titer which has not been effectively cleared due to a defective or inadequate host immune response. If defective clearance is responsible for the viral titer profile observed, then treatment with antivirals late in the infection will have little effect on the morbidity of the infection. In fact, treatment would likely contribute to increasing drug resistance, and the defective clearance would increase

the chances of propagation of the lingering drug-resistant virions. On the other hand, if sustained viral production is responsible for the observed viral titer profile, as is the case in our two target cell model, this would provide us with a longer time window where treatment with antivirals would have beneficial effects in reducing disease morbidity.

Late treatment with the neuraminidase inhibitor oseltamivir has little or no effect on infection severity for infections with human-adapted seasonal influenza strains [1, 34]. This is because viral titer peaks early ($\sim$ 2 dpi) for seasonal influenza infections and by then treatment with neuraminidase inhibitors, which block viral release from infected cells, has almost no viral release left to block. However, if viral production peaks later and is sustained for several days, as in our two target cell model and as suggested by experimental data [16, 78], treatment with neuraminidase inhibitors, even if applied late in the infection, could significantly reduce morbidity. This was seen in patients infected with avian influenza strains for whom treatment with oseltamivir was initiated late (4–8 dpi) but resulted in $\sim$100-fold decreases in viral titers compared to patients who had developed drug-resistance [18].

The two target cell model has a threshold for the secondary cell population, analogous to the basic reproductive number, below which infection is restricted to spread only through the default cell population and above which the secondary cell population will also fall prey to the infection. The severe infections characterized by a sustained viral production in our two cell model are located near that parameter threshold. Thus, our model predicts that small reductions in either the secondary cells' susceptibility to infection or production rate of virus, as can be achieved through treatment with adamantanes or neuraminidase inhibitors, respectively, could have a sharp and significant effect on infection severity and the duration of the symptomatic infection.

It is important to note that there are certain limitations to our current approach. Our model assumes that cells of the two types are uniformly distributed in space. The effect of spatial heterogeneity on the dynamics of infection may be worthwhile to consider, as the

distribution of ciliated and non-ciliated cells may change in different regions of the respiratory tract [79]. A gradient switching progressively from a mostly ciliated to a mostly non-ciliated cell population rather than a uniform distribution might be more appropriate. The dynamics of influenza infection have been shown to be sensitive to different spatial distributions of initially infected cells [4]. This may have important implications for the outcome of infection within a two target cell population.

In addition, to accurately model the spread of in-host viral infections, the host immune response must be taken into account. Due to the relatively short duration of seasonal influenza infections, it might be reasonable to ignore or not explicitly take into consideration the role of host immunity. But infections with high viral loads over extended periods, such as those predicted by our model, will likely elicit a stronger and therefore more destructive immune response than infections which are cleared early. High levels of chemokines and cytokines have indeed been detected in patients infected with the influenza A (H5N1) virus [16, 83]. The release of cytokines shortly after viral infection, in what is known as a "cytokine storm", is believed to be one of the underlying causes for the high morbidity in patients infected with the influenza A (H5N1) strains [9]. Furthermore, as a patient is infected for longer periods of time, the adaptive immune response will begin to play a significant role in the infection dynamics. Attempts to incorporate the immune response into our model will certainly aid in our understanding of the immune response to severe influenza infections; however, the inclusion of additional parameters for the immune response must be justified with a sufficient amount of experimental data which are not currently available.

While differences in severity between human- and avian-derived influenza strains likely depend on several factors, we have demonstrated that a difference in cell tropism alone can be sufficient to explain or at least to capture the important differences in severity between these two strain subtypes. This makes the two target cell model a useful tool for studying delayed antiviral treatment of infections characterized by sustained viral production. In

addition, since our model is a simple extension of the classic viral dynamics model used to capture in-host infection with a variety of other diseases such as HIV [71, 72], and Hepatitis viruses [57, 61, 65, 66], our conclusions also apply to these other diseases where different cell types can be affected by the virus.

Chapter 5

Parameter rescaling of the two-cell model

5.1 Introduction

In the previous chapter, the effect of changing the scaling parameters r_p and r_β was investigated for a population of two different target cells. It was found that the quantities R_s and R_d determine if the infection will spread within the two different cell populations. However, the only parameters that were allowed to vary between the two different cell populations were the scaling parameters r_p and r_β. Therefore, it is not known if the kinetics of the infection are dependent on the values of R_s and R_d alone irrespective of the value of the individual parameters, or if changing the default model parameters while keeping R_s and R_d constant will change the dynamics of the infection.

To investigate this matter more closely, we repeated the analysis of the measures of disease severity completed in the previous chapter (i.e. time of viral titer peak and total virus produced) but this time we allowed each of the other model parameters to vary individually while keeping R_s and R_d constant. In our analysis, we find that rescaling the model param-

eters can change the dynamics of infection; however, the long-lasting, high viral loads found in the previous chapter are still present.

5.2 Methods

We vary the proportion of secondary target cell from r_T (pre-scaling) to r'_T (post-scaling) and rescale other model parameters so as to keep R_s and R_d constant despite the change in r_T. This is done through the use of two rescaling parameters, α and λ, such that

$$R_d = \underbrace{\frac{\beta p(1-r_T)T_0}{\delta c}}_{\text{pre-scaling}} = \underbrace{\alpha\frac{\beta p(1-r'_T)T_0}{\delta c}}_{\text{post-scaling}}$$

and

$$R_s = \underbrace{\frac{(r_\beta\beta)(r_p p)(r_T T_0)}{\delta c}}_{\text{pre-scaling}} = \underbrace{\alpha\lambda\frac{(r_\beta\beta)(r_p p)(r'_T T_0)}{\delta c}}_{\text{post-scaling}}.$$

where the equality requires that

$$\alpha = \frac{(1-r_T)}{(1-r'_T)},$$

and

$$\lambda = \frac{1}{\alpha}\frac{r_T}{r'_T}.$$

By applying α to r_β so that r_β becomes αr_β post-scaling, we can explore the effect of varying each parameter individually, such as p pre-scaling becoming λp post-scaling, and so on for each of the parameters. Specifically, in our analysis we set $r_T = 0.4$ and $r'_T = 0.2$, such that r_β is rescaled to $(3/4)\beta$ and $\lambda = 8/3$ is applied to either β, p, δ or c. To quantify this rescaling, we use the equation

$$R = \frac{N_{\text{pre}} - N_{\text{post}}}{N_{\text{pre}}}, \tag{5.1}$$

where N is the measure of disease severity we wish to compare (e.g. time of viral titer peak) in the different cases.

5.3 Results

The effect of rescaling on the time of viral titer peak and on the amount of virus produced are illustrated in Figures 5.1 and 5.2, respectively. In Figure 5.1, we note that similar effects are found when δ and c are rescaled, while rescaling β and p leads to small changes for $R_s < 1$ only. For the parameter rescalings in Figure 5.1, the viral titer will peak at approximately the same time as the viral titer peak for the base case, regardless of which parameter is rescaled. This change is small for most regions of the parameter space. However, the time of viral titer peak for the rescaled parameters changes significantly near the region $R_s = 1$ when any of the parameters are rescaled. This demonstrates that small parameter changes can lead to large changes in the infection dynamics just past the threshold $R_s = 1$.

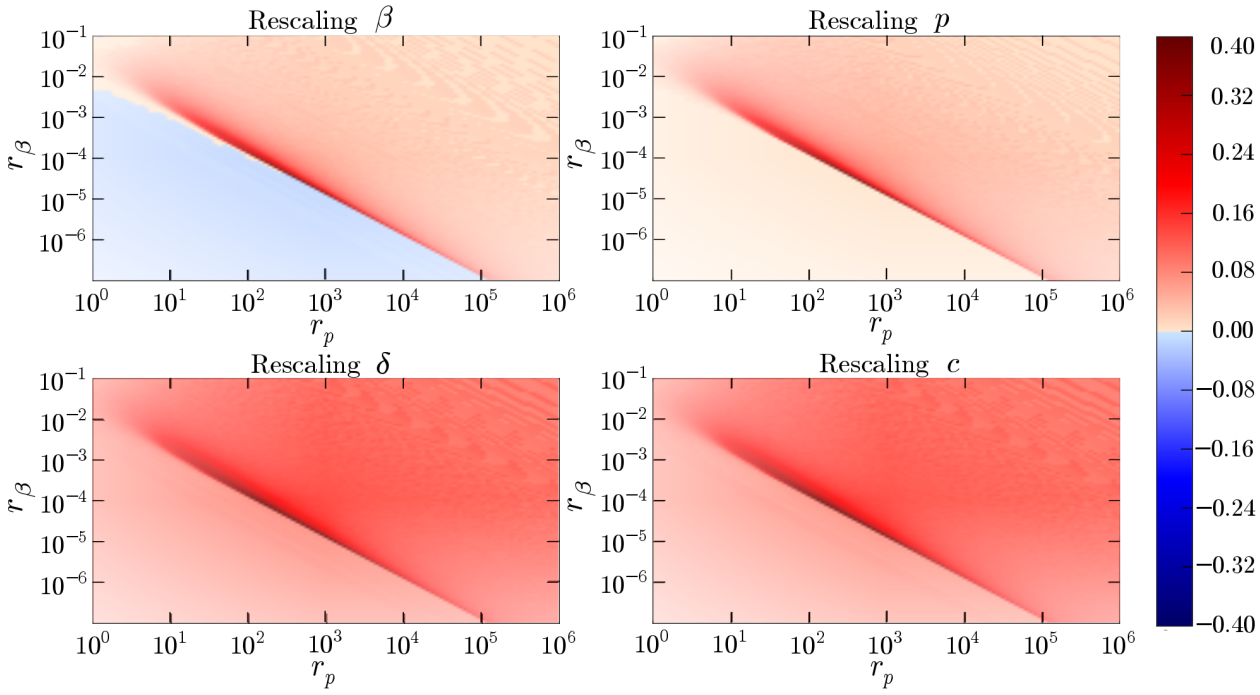

Figure 5.1 Effect of rescaling on time of viral load peak. Rescaling so as to keep R_s, R_d the same pre- and post-scaling was done by rescaling $r_\beta \to \lambda r_\beta$, and the parameter indicated above the respective graph by a constant factor α.

When the difference in amount of virus produced is considered, we note that decreasing

the rate of of viral production, p, and decreasing the infected cell lifespan, $1/\delta$, has the same effect on the amount of virus produced, while decreasing the rate of infection, β, and increasing the viral clearance rate, c, also has the same effect on virus produced. This is demonstrated in Figure 5.2. A sharp boundary is located at the threshold $R_s = 1$; the amount of virus produced, relative to the base case, decreases significantly once this threshold is surpassed, due to the secondary cells' contribution to the infection.

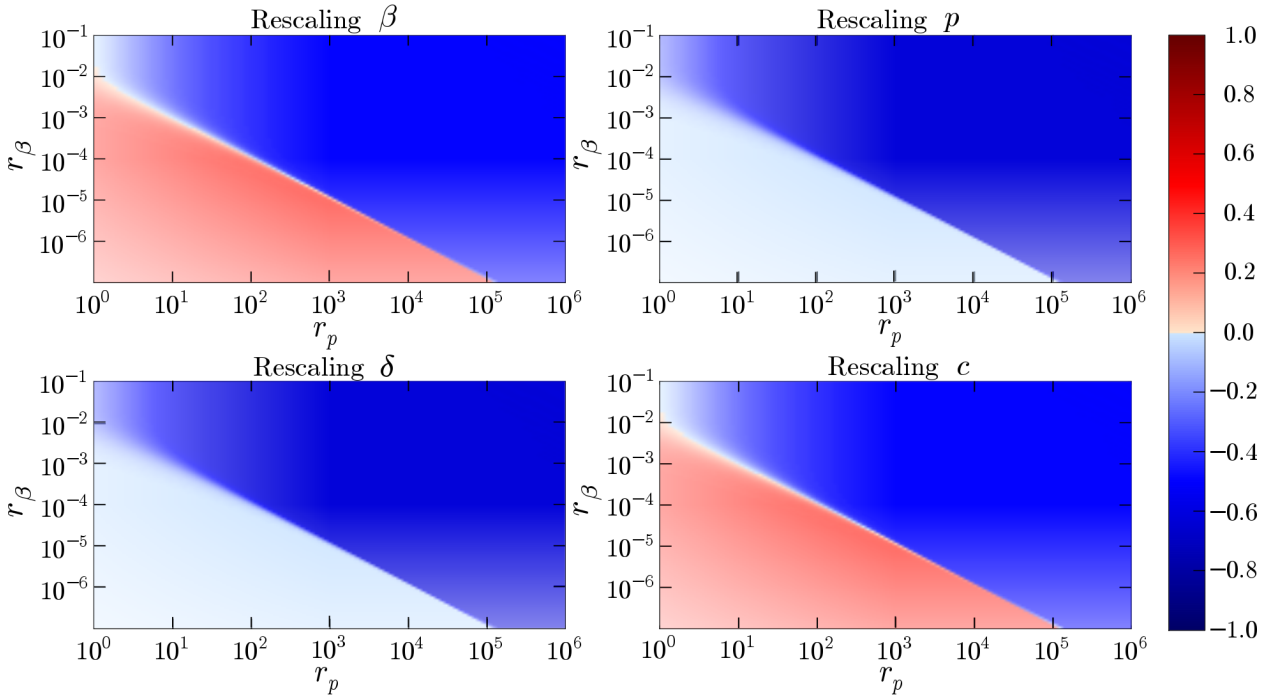

Figure 5.2 Effect of rescaling on total amount of virus produced. Rescaling so as to keep R_s, R_d the same pre- and post-scaling was done by $r_\beta \to \lambda r_\beta$, and the parameter indicated above the respective graph by a constant factor α.

The effects of rescaling the parameter r_p such that r_p pre-scaling becomes λr_p post-scaling rather than the parameter r_β were also investigated. The results were similar to the case when r_β is rescaled; however, no large variations were found near the threshold $R_s = 1$; instead, the changes from the base case were uniform throughout the parameter space. This suggests that rescaling the parameter r_β is important when considering rescaling effects.

We also considered how rescaling the parameter k, which represents the rate of transition from a latently infected to productively infected cell, affects the results found in the previous chapter. As this parameter is not represented in the quantities R_s or R_d, no other parameters were rescaled in conjunction with k. We found that decreasing k (and therefore increasing the length of latent infection, $1/k$) led to a later peak of the viral titer, relative to the base case, while shortening the length of latent infection led to an earlier time for the viral titer peak. These results are not surprising, as decreasing the rate of transition from a latently infected to productively infected cell leads to an increased overall lifespan of the infected cell, and vice versa.

The effect on the total amount of virus produced when the length of latent infection, k, is varied was also investigated. Changing this parameter has no effect on the total amount of virus produced for the total duration of infection; only the delay after a susceptible cell is infected, but before virus begins to be produced, will change. Therefore, the viral titer will peak at a different time, depending on how k is rescaled. Additionally, we expect the same amount of virus to be produced, regardless of the value of k, and this is indeed what was found.

5.4 Discussion

In the previous chapter, a threshold for infection within each cell population was found which determined if the infection would spread to the secondary cell population. This threshold is comprised of several of the default parameter values from equations (4.1). We looked at the effect of changing the default parameter values, while keeping the quantities R_d and R_s constant, to see if the dynamics of infection change.

It was found that rescaling individual parameters, while keeping the infection thresholds R_s and R_d constant, did not change the general dynamics of infection (i.e. the region with sustained viral titer). However, the length of infection and amount of virus produced changed

when individual parameters were rescaled. These changes were most significant near the infection threshold $R_s = 1$, suggesting small parameter variations can lead to large changes near this region.

We also found that rescaling different parameters can lead to similar effects on the measures of disease severity. For the time of viral titer peak, rescaling the rates of infected cell death and viral clearance have similar effects on the dynamics of infection. Similarly, for the amount of virus produced, rescaling the rates of viral production and cell death produces similar infection dynamics, while rescaling the rates of infectivity and viral clearance also produce similar results. This suggests that there may be underlying mathematical or biological relationships between these parameters.

We also looked at how changing the rate of transition from latently infected cell to a productively infected cell changes the dynamics. When changing this parameter, the infection thresholds R_d and R_s did not need to be rescaled, as the rate of transition does not appear in these thresholds. It was found that the longer it takes an infected cell to transition to a productively infected cell, the later the viral titer will peak. It was found that the same amount of virus was produced throughout the course of infection, regardless of how the rate of transition was rescaled.

In conclusion, our analysis confirms that the infection thresholds $R_s = 1$ and $R_d = 1$ hold, regardless of the parameter values used to obtain these thresholds. However, rescaling these parameters still leads to changes of the infection dynamics, especially around the region $R_s = 1$. Changes to certain parameters also led to redundancy in the measures of disease severity, when compared to a default case. In summary, our conclusion that long-lasting infection with sustained viral titer is produced with this model, and that the infection threshold R_s defines when these dynamics occur, still holds.

Chapter 6

Conclusion

Mathematical models have yielded important insights into the behaviour of within-host viral infections. Recent progress in modelling of influenza infection dynamics has demonstrated that simple models can provide valuable insight into infections which can supplement experimental results. However, these models fail to capture the dynamics of in-host infections with highly virulent influenza strains, which appear to last longer than seasonal influenza infections and lead to higher viral titers.

In this thesis, a mathematical model was used to explain the behaviour of in-host infections with highly virulent influenza strains. Using the assumption that different strains of influenza virus preferentially bind to and infect different types of cells in the respiratory tract, we investigated whether cell tropism could explain why certain influenza strains result in more severe infection than seasonal influenza strains which are well adapted to their human hosts. The model is an extension of a simpler model of influenza infection used to successfully explain experimental data for human infections with a seasonal influenza strain [1].

The results of our analysis suggest that our model is sufficient to explain the dynamics of highly virulent influenza infection. The infection is characterized by high levels of viral titer which peak long after infection is initiated, relative to seasonal influenza infections. In

our model, the viral titer is also sustained at high levels for long periods of time, which is believed to be a characteristic of highly virulent viral strains.

Our analysis has also yielded a quantity, analogous to the basic reproductive number in infectious disease dynamics, which determines if an infection will spread through a population of cells. Using this quantity, we found that the type of behaviour exhibited by highly virulent strains develops when the infection spreads rapidly through one cell population, then spreads at a much slower rate through the second cell population. This infection threshold is especially important for analyzing infections of more than one cell type, each with different parameters, as this threshold quantifies how efficient the virus is in spreading to different cell populations. We also investigated whether the model's behaviour is robust to changes in parameter values, i.e whether the infection threshold holds in a more general case within our model, where we rescale the default parameter values. This analysis showed that while certain characteristics of the infection may be changed by rescaling parameters, such as the time of viral peak, the infection threshold is still present over a wide range of parameter values and remains key to determining if an infection will exhibit long-lasting, high levels of viral titer.

The presence of high levels of viral titer sustained over long periods provides the opportunity to increase our understanding of the mechanisms used to fight influenza infections. The long-lasting infection exhibited in our analysis is associated with an increased morbidity in humans and animals [50, 56, 68] and decreasing the duration of infection may lead to higher survival rates. By explicitly introducing an immune response or antiviral drug treatment into the model, a better understanding of how these mechanisms reduce infection morbidity may be gained, along with the ability to optimize antiviral drug treatment regimes. In a recently submitted paper [20], this model was used to estimate the efficacy of antiviral drugs during infection with avian influenza strains. The results suggest that delayed treatment (> 2 dpi) with antiviral drugs can significantly reduce the duration of infection for avian

derived strains, while delayed treatment of human strains has little effect on the infection duration.

The model discussed here, while providing valuable insight into the dynamics of highly virulent viruses, is a starting point for more fruitful research in this area. By considering extensions of this model, a greater understanding of the mechanisms behind the disease may be gained. The mathematical analysis of influenza infections is still in its infancy, and there is a vast amount that is yet to be understood. Through the efforts of modelling this disease, our understanding of influenza infection dynamics will continue to grow for the foreseeable future.

Bibliography

[1] P. Baccam, C.A.A. Beauchemin, C. A. Macken, F. G. Hayden, and A. S. Perelson. Kinetics of influenza A virus infection in humans. *J. Virol.*, 80(15):7590–7599, August 2006.

[2] S. H. Bajaria, G. Webb, M. Cloyd, and D. Kirschner. Dynamics of naive and memory CD4+ T lymphocytes in HIV-1 disease progression. *JAIDS*, 30(1):41–58, May 1 2002.

[3] A.L Bauer, C.A.A Beauchemin, and A.S Perelson. Agent-based modeling of host-pathogen systems: The successes and challenges. *Information Sciences*, 179:1379–1389, 2008.

[4] C.A.A. Beauchemin. Probing the effects of the well-mixed assumption on viral infection dynamics. *J. Theor. Biol.*, 242(2):464–477, 21 September 2006. Draft available on arXiv:q-bio.CB/0505043.

[5] C.A.A. Beauchemin, J.J McSharry, G.L Drusano, J.T Nguyen, G.T Went, R.M Ribeiro, and A.S Perelson. Modeling amantadine treatment of influenza A virus in vitro. *J. Theor. Biol.*, 254:439–451, 2008.

[6] G. A. Bocharov and A. A. Romanyukha. Mathematical model of antiviral immune response III. Influenza A virus infection. *J. Theor. Biol.*, 167(4):323–360, 1994.

[7] S. Bonhoeffer, R. M. May, G. M. Shaw, and M. A. Nowak. Virus dynamics and drug therapy. *PNAS*, 94:6971–6976, 1997.

[8] M.C.W. Chan, C.Y Cheung, W. H. Chui, S.W. Tsao, J.M. Nicholls, Y.O. Chan, R.W.Y. Chan, H.T. Long, L.L.M. Poon, Y. Guan, and J.S.M. Peiris. Proinflammatory cytokine responses induced by influenza A (H5N1) viruses in primary human alveolar and bronchial epithelial cells. *Respir. Res.*, 6:135, 11 November 2005.

[9] C.Y Cheung, L. L. M. Poon, A. S Lau, W. Luk, Y. L. Lauand K. F Shortridge, S. Gordon, Y. Guan, and J .S. M. Peiris. Induction of proinflammatory cytokines in human macrophages by influenza A (H5N1) viruses: A mechanism for the unusual severity of human disease? *Lancet*, 360(9348):1831–1837, 7 December 2002.

[10] T. K. W. Cheung and L. L. M Poon. Biology of influenza A virus. *Ann. N.Y Acad. Sci.*, 1102(1):1–25, April 2007.

[11] R.A. Childs, A.S. Palma, S. Wharton, T. Matrosovich, Y. Liu, W. Chai, M.A. Campanero-Rhodes, Y. Zhang, M. Eickmann, M. Kiso, A. Hay, M. Matrosovich, and T. Feizi. Receptor-binding specificity of pandemic influenza a (H1N1) 2009 virus determined by carbohydrate microarray. *Nat. Biotechnol.*, 27(9):797–799, September 2009.

[12] T. Chotpitayasunodh, K. Ungchusak, W. Hanshaoworakul, S. Chunsuthiwat, P. Sawanpanyalert, R. Kijphati, S. Lochindarat, P. Srisan, P. Suwan, Y. Osotthanakorn, T. Anatasetagoon, S. Kanjanawasri, S. Tanupattarachai, J. Weerakul, R. Chaiwirattana, M. Maneerattanaporn, R. Poolsavatkitikool, K. Chokephaibulkit, A. Apisarnthanarak, and S. Dowell. Human disease from influenza A (H5N1), Thailand, 2004. *Emerging Infectious Diseases*, 11(2):201–209, February 2005.

[13] R. Coombes. Doctors call for guidance on how to prioritise critically ill patients in swine flu pandemic. *BMJ*, 339:b3092, 29 July 2009.

[14] R. G. Crystal and J. B. West. *The Lung: Scientific Foundations*. Raven Press Ltd., New York, USA, 1991.

[15] H. Dahari, A. Feliu, M. Garcia-Retortillo, X. Forns, and A. U. Neumann. Second hepatitis C replication compartment indicated by viral dynamics during liver transplantation. *J. Hepatol*, 42:491–498, January 2005.

[16] M. D. de Jong, C. P. Simmons, T. T. Thanh, V. M. Hien, G. J. D. Smith, T. N. B. Chau, D. M. H., N. V. V. Chau, T. H. Khanh, V. C. Dong, P. T. Qui, B. Van Cam, D. Quang Ha, Y. Guan, J. S. Malik Peiris, N. T. Chinh, T. T. Hien, and J. Farrar. Fatal outcome of human influenza A (H5N1) is associated with high viral load and hypercytokinemia. *Nat. Med.*, 12(10):1203–1207, October 2006.

[17] M. D. de Jong, C. P. Simmons, T. T. Thanh, V. M. Hien, G. J. D. Smith, T. N. B. Chau, D. M. Hoang, N. V. V. Chau, T. H. Khanh, V. C. Dong, P. T. Qui, B. V. Cam, D. Q. Ha, Y. Guan, J. S. Malik Peiris, N. T. Chinh, T. T. Hien, and J. Farrar. Fatal avian influenza A (H5N1) in a child presenting with diarrhea followed by coma. *N. Engl. J. Med*, 352(7):686–691, February 17 2005.

[18] M. D. de Jong, T. T. Thanh, T. H. Khanh, V. M. Hien, G. J.D. Smith, N. Vinh Chau, B. V. Cam, P. T. Qui, D. Q. Ha, Y. G., J.S. M. Peiris, T. T. Hien, and J. Farrar. Oseltamivir resistance during treatment of influenza A (H5N1) infection. *N Engl. J. Med.*, 353(25):2667–2672, 22 December 2005.

[19] O. Diekmann, J. A. P. Heesterbeek, and J. A. J. Metz. On the definition and the computation of the basic reproduction ratio R_0 in models for infectious diseases in heterogeneous populations. *J. Math. Biol.*, 28(4):365–382, 1990.

[20] H. M. Dobrovolny, R. Gieschke, B. Davies, N. L. Jumbe, and C. A. A. Beauchemin. Neuraminidase inhibitors for treatment of human and avian strain influenza: A comparative modelling study. *Submitted*, 2009.

[21] J. W. Drake. Rates of spontaneous mutation among RNA viruses. *Proc. Natl. Acad. Sci. USA*, 90(9):4171–4175, 1 May 1993.

[22] J. W. Eaton et al. *GNU Octave version 3.0.1*, 2008. A free open-source software for solving linear and nonlinear problems numerically, and for performing other numerical experiments using a language that is mostly compatible with Matlab. Available at: `http://www.octave.org`.

[23] P. Eizenberg. The general practice experience of the swine flu epidemic in Victoria — lessons from the front line. *Med. J. Aust.*, 191(3):151–153, 3 August 2009.

[24] R. S. Fritz, F. G. Hayden, D. P. Calfee, L. M. R. Cass, A. W. Peng, W. G. Alvord, W. Strober, and S. E. Straus. Nasal cytokine and chemokine response in experimental influenza A virus infection: Results of a placebo-controlled trial of intravenous zanamivir treatment. *J. Infect. Dis.*, 180:586–593, 1999.

[25] W. R. Gallaher. Towards a sane and rational approach to management of influenza H1N1 2009. *Virol. J.*, 6(1), 7 May 2009.

[26] V. V. Ganusov, C. T. Bergstrom, and R. Antia. Within-host population dynamics and the evolution of microparasites in a heterogeneous host population. *Evolution*, 56(2):213–223, 2002.

[27] P. Gao, S. Watanabe, T. Ito, H. Goto, K. Wells, M. McGregor, A. J. Cooley, and Y. Kawaoka. Biological heterogeneity, including systemic replication in mice, of H5N1 influenza A virus isolates from humans in Hong Kong. *J. Virol.*, 73(4):3184–3189, April 1999.

[28] Richard A. Goldsby, Thomas J. Kindt, and Barbara A. Osborne. *Kuby Immunology* 4^{th} *Edition*. W. H. Freeman and Company, New York, 2000.

[29] C. B. Hall. The spread of influenza and other respiratory viruses: complexities and conjectures. *Clinical Infectious Diseases*, 45:353–359, 2007.

[30] B. Hancioglua, D. Swigona, and G. Clermont. A dynamical model of human immune response to influenza A virus infection. *J. Theor. Biol.*, 246(1):70–86, 7 May 2007.

[31] A. Handel, I. M. Longini Jr., and R. Antia. Neuraminidase inhibitor resistance in influenza: Assessing the danger of its generation and spread. *PLoS Comput. Biol.*, 3(12):0001–0009, December 2007.

[32] A. Handel, I. M. Longini Jr., and R. Antia. Towards a quantitative understanding of the within-host dynamics of influenza a infections. *J. R. Soc. Interface*, page published online, May 27 2009.

[33] F. G. Hayden, R. S. Fritz, M. C. Lobo, W. G. Alvord, W. Strober, and S. E. Strauss. Local and systemic cytokine responses during experimental human influenza A virus infection. *J. Clin. Invest.*, 101(3):643–649, February 1998.

[34] F. G. Hayden, J. J. Treanor, R. F. Betts, M. Lobo, J. D. Esinhart, and E. K. Hussey. Safety and efficacy of the neuraminidase inhibitor GG167 in experimental human influenza. *JAMA*, 275(4):295–299, January 1996.

[35] J.M. Heffernan, R.J. Smith, and L.M. Wahl. Perspectives on the basic reproductive ratio. *J. R. Soc. Interface*, 4(2):281–293, 22 September 2005.

[36] H. W. Hethcote and J. W. van Ark. Epidemiological models for heterogeneous populations: Proportionate mixing, parameter estimation and immunization programs. *Math. Biosci.*, 84:85–118, 1987.

[37] A.C. Hindmarsh. ODEPACK, a systematized collection of ODE solvers. In R.S. Stepleman et al., editors, *IMACS Transactions on Scientific Computation*, volume 1, pages 55–64. North-Holland, Amsterdam, 1983.

[38] S-M. Hsieh and S-C. Chang. Insufficient perforin expression in CD8+ T cells in response to hemagglutinin from avian influenza (H5N1) virus. *J. Immunol.*, 176(8):4530–4533, 15 April 2006.

[39] A. Ibrecevic, A. Pekosz, M. J. Walter, C. Newby, J. T. Battaile, E. G. Brown, M. J. Holtzman, and S. L. Brody. Influenza virus receptor specificity and cell tropism in mouse and human airway epethilial cells. *J. Virol.*, 80(15):7469–7480, August 2006.

[40] N. P. A. S. Johnson and J. Mueller. Updating the accounts: Global mortality of the 1918-1920 Spanish influenza pandemic. *Bull. Hist. Med.*, 76(1):105–15, Spring 2001.

[41] L. Kaiser, R. S. Fritz, S. E. Strauss, L. Gubareva, and F. Hayden. Symptom pathogenesis during acute influenza: Interleukin-6 and other cytokine responses. *J. Med. Virol.*, 64:262–268, 2001.

[42] M. A. Kaufman, G. J. Duke, F. McGain, C. French, C. Aboltins, G. Lane, and G. A. Gutteridge. Life-threatening respiratory failure from H1N1 influenza 09 (human swine influenza). *Med. J. Aust.*, 191(3):154–156, 3 August 2009.

[43] T. Kogure, T. Suzuki, T. Takahashi, D. Miyamoto, K. I.P.J Hidari, C-T. Guo, T. Ito, Y. Kawaoka, and Y. Suzuki. Human trachea primary epithelial cells express both sialyl(α2-3)Gal receptor for human parainfluenza virus type 1 and avian influenza viruses, and sialyl(α2-6)Gal receptor for human influenza virus. *Glycoconj. J.*, 23(1–2):101–106, February 2006.

[44] E.W. Larson, J.W. Dominik, A.H. Rowberg, and G.A. Higbee. Influenza virus population dynamics in the respiratory tract of experimentally infected mice. *Infect. Immun.*, 13(2):438–447, February 1976.

[45] R. C. Larson. Simple models of influenza progression within a heterogeneous population. *Op. Res.*, 55(3):399–412, May-June 2007.

[46] H. Y. Lee, D. J. Topham, S. Y. Park, J. H., J. Treanor, T. R. Mosmann, X. Jin, B. M. Ward, H. Miao, J. Holden-Wiltse, A. S. Perelson, M. Zand, and H. Wu. Simulation and prediction of the adaptive immune response to influenza virus infection. *J. Virol.*, 83(14):7151–7165, July 2009.

[47] A. S. Lipatov, S. Andreansky, R. J. Webby, D. J. Hulse, J. E. Rehg, S. Krauss, D. R. Perez, P. C. Doherty, R. G. Webster, and M. Y. Sangster. Pathogenesis of Hong Kong H5N1 influenza virus NS gene reassortants in mice: The role of cytokines and B- and T-cell responses. *J. Gen. Virol.*, 86:1121–1130, 2005.

[48] A. S. Lipatov, Y. K. Kwon, L. V. Sarmento, K. M. Lager, E. Spackman, D. L. Suarez, and D. E. Swayne. Domestic pigs have low susceptibility to H5N1 highly pathogenic avian influenza viruses. *PLoS Pathog.*, 4(7):1–10, 11 July 2008.

[49] T. R. Maines, L-M. Chen, Y. Matsuoka, H. Chen, T. Rowe, J. Ortin, A. Falcon, N. T. Hien, L. Q. Mai, E. R. Sedyaningsih, S. Harun, T. M. Tumpey, R. O. Donis, N. J. Cox, K. Subbarao, , and J. M. Katz. Lack of transmission of H5N1 avian human reassortant influenza viruses in a ferret model. *PNAS*, 103(32):12121–12126, 8 August 2006.

[50] T. R. Maines, A. Jayaraman, J. A. Belser, D. A. Wadford, C. Pappas, H. Zeng, K. M. Gustin, M. B. Pearce, K. Viswanathan, Z. H. Shriver, R. Raman, N. J. Cox, R. Sasiekharan, J. M. Katz, and T. M. Trumpey. Transmission and pathogenesis of swine-origin 2009 A(H1N1) influenza viruses in ferrets and mice. *Science*, 325:484–487, 24 July 2009.

[51] M. N. Matrosovich, T. Y. Matrosovich, T. Gray, N. A. Roberts, and H-D. Klenk. Human and avian influenza viruses target different cell types in cultures of human airway epithelium. *P. Natl. Acad. Sci. USA*, 101(13):4620–4624, 30 March 2004.

[52] M. N. Matrosovich, T. Y. Matrosovich, T. Gray, N. A. Roberts, and H-D. Klenk. Neuraminidase is important for the initiation of influenza virus infection in human airway epithelium. *J. Virol.*, 78(22):12665–12667, Nov. 2004.

[53] M. N. Matrosovich, T. Y. Matrosovich, J. Uhlendorff, W. Garten, and H-D. Klenk. Avian-virus-like receptor specificity of the hemagglutinin impedes influenza virus replication in cultures of human airway epithelium. *Virology*, 361(2):384–390, 10 May 2007.

[54] M. A. Mohsin, S. J. Morris, H. Smith, and C. Sweet. Correlation between levels of apoptosis, levels of infection and haemagglutinin receptor binding interaction of various subtypes of influenza virus: does the viral neuraminidase have a role in these associations. *Virus Research*, 85:123–31, 2002.

[55] H. Motulsky and A. Christopoulos. *Fitting Models to Biological Data Using Linear and Nonlinear Regression: A practical guide to curve fitting.* Oxford, New York, 2004.

[56] V. J. Munster, E. de Wit, J. M. A. van den Brand, S. Herfst, E. J.A. Schrauwen, T. M. Bestebroer, D. van de Vivjer, C. A. Boucher, M. Koopmans, G. F. Rimmelzwaan, T. Kuiken, A. D. M. E. Osterhaus, and R. A. M. Fouchier. Pathogenesis and transmission of swine-origin 2009 A(H1N1) influenza virus in ferrets. *Science*, 325:481–483, 24 July 2009.

[57] A. U. Neumann, N. P. Lam, H. Dahari, D. R. Gretch, T. E. Wiley, T. J. Layden, and A. S. Perelson. Hepatitis C viral dynamics in vivo and the antiviral efficacy of interferon-α therapy. *Science*, 282(5386):103–107, 2 October 1998.

[58] J.M Nicholls, M.C.W Chan, W.Y Chan, H.K Wong, C.Y Cheung, D.W.W Kwong, M.P Wong, W.H Chui, L.L.M.Poon, S.W Tsao, Y.Guan, and J.S.M Peiris. Tropism of avian influenza A H5N1 in the upper and lower respiratory tract. *Nature Medicine*, 13(2):147–149, 2007.

[59] Novel Swine-Origin Influenza A (H1N1) Virus Investigation Team. Emergence of a novel swine-origin influenza A (H1N1) virus in humans. *N. Engl. J. Med.*, 360(25):2605–2615, 18 June 2009.

[60] M. A. Nowak and R. M. May. *Virus Dynamics: Mathematical Principles of Immunology and Virology*. Oxford University Press, Oxford, 2000.

[61] M.A. Nowak, S. Bonhoeffer, A.M. Hill, R. Boehme, H.C Thomas, and H. McDade. Viral dynamics in hepatitis B viral infection. *Proc. Natl. Acad. Sci. USA*, 93:4398–4402, April 1996.

[62] Writing Committee of the Second World Health Organization Consultation on Clinical Aspects of Human Infection with Avian Influenza A (H5N1) Virus. Update on avian influenza A (H5N1) virus infection in humans. *N. Engl. J. Med.*, 358:261–273, 17 January 2008.

[63] The Writing Committee of the World Health Organization WHO Consultation on Human Influenza A/H5. Avian influenza A (H5N1) infection in humans. *N. Engl. J. Med.*, 353:1374–1385, September 29 2005.

[64] R.J. Pack, Layla H. A1-Ugaily, G. Morris, and J.G. Widdicombe. The distribution and structure of cells in the tracheal epithelium of the mouse. *Cell Tissue Res.*, 208:65–84, 1980.

[65] R. J. H. Payne, M. A. Nowak, and B. S. Blumberg. Analysis of a cellular model to account for the natural history of infection by the hepatitis B virus and its role in the development of primary hepatocellular carcinoma. *J. Theor. Biol.*, 159:215–240, 1992.

[66] R. J. H. Payne, M. A. Nowak, and B. S. Blumberg. A cellular model to explain the pathogenesis infection by the hepatitis B virus. *Math. Biosci.*, 123:25–58, 1994.

[67] J. S. M Peiris, W. C. Yu, C. W. Leung, C. Y Cheung, W. F. Ng, J. M Nicholls, T. K Ng, K. H Chan, S. T Lai, W. K. Lim qand K. Y Yuen, and Y. Guan. Re-emergence of fatal human influenza a subtype H5N1 disease. *Lancet*, 363(9409):617–619, 2004.

[68] J.S. Malik Peiris, M. D. de Jong, and Y. Guan. Avian influenza virus H5N1: a threat to human health. *Clin. Microbiol. Rev.*, 20(2):243–267, 2007.

[69] A. Pekosz, C. Newby, P. S. Bose, and A. Lutz. Sialic acid recognition is a key determinant of influenza A virus tropism in murine trachea epithelial cell cultures. *Virology*, 386:61–67, 2009.

[70] A. S. Perelson. Modelling viral and immune system dynamics. *Nature Rev. Immunol.*, 2(1):28–36, 2002.

[71] A. S. Perelson, P. Essunger, Y. Cao, M. Vesanen, A. Hurley, K. Saksela, M. Markowitz, and D. D. Ho. Decay characteristics of HIV-1 infected compartments during combination therapy. *Nature*, 387(6629):188–191, 8 May 1997.

[72] A. S. Perelson, A.U. Neumann, M. Markowitz, J.M. Leonard, and D.D. Ho. HIV-1 dynamics *in vivo*: Virion clearance rate, infected cell life-span, and viral generation time. *Science*, 271(5255):1582–1586, 15 March 1996.

[73] L. A. Perrone, J. K. Plowden, A. Garca-Sastre, J. M. Katz, and T. M. Tumpey. H5N1 and 1918 pandemic influenza virus infection results in early and excessive infiltration of

macrophages and neutrophils in the lungs of mice. *PLoS Pathog.*, 4(8):1–11, 1 August 2008.

[74] G. F. Rimmelzwaan, N. J. Nieuwkoop, G. de Mutsert, A. C.M. Boon, T. Kuiken, R. A.M. Fouchier, and A. D.M.E. Osterhaus. Attachment of infectious influenza A viruses of various subtypes to live mammalian and avian cells as measured by flow cytometry. *Virus Res.*, 129:175–181, 22 August 2007.

[75] G.N. Rogers, J.C. Paulson, R.S. Daniels, J.J Skehel, I.A. Wilson, and D.C Wiley. Single amino acid substitutions in influenza haemagglutinin change receptor binding specificity. *Nature*, 304:76–78, 7 July 1983.

[76] G. A. Frederick Seber and C. J. Wild. *Nonlinear Regression.* John Wiley & Sons, Inc., New York, USA, 1989.

[77] S. H. Seo, E. Hoffmann, and R. G. Webster. Lethal H5N1 influenza viruses escape host anti-viral cytokine responses. *Nature Med.*, 8(9):950–954, September 2002.

[78] S. H. Seo and R. G. Webster. Tumor necrosis factor alpha exerts powerful anti-influenza virus effects in lung epithelial cells. *J. Virol.*, 76(3):1071–1076, February 2002.

[79] K. Shinya, M. Ebina, S. Yamada, M. Ono, N. Kasai, and Y. Kawaoka. Influenza virus receptors in the human airway. *Nature*, 440(7083):435–436, 23 March 2006.

[80] A. M. Smith, F. R. Adler, and A. S. Perelson. An accurate two-phase approximate solution to an acute viral infection model. *J. Math. Biol.*, in press, 2009. doi:10.1007/s00285-009-0281-8.

[81] J. Stevens, O. Blixt, L-M. Chen, R. O. Donis, J. C. Paulson, and I. A. Wilson. Recent avian H5N1 viruses exhibit increased propensity for acquiring human receptor specificity. *J. Mol. Biol.*, 381(5):1382–1394, 18 September 2008.

[82] C. I. Thompson, W. S. Barclay, M. C. Zambon, and R. J. Pickles. Infection of human airway epithelium by human and avian strains of influenza A virus. *J. Virol.*, 80(16):8060–8068, August 2006.

[83] K-F. To, P. K. S Chan, K-F. Chan, W-K. Lee, W-Y. Lam, K-F. Wong, N. L. S Tang, D. N. C Tsang, R. Y. T Sung, T. A. Buckley, J. S. Tam, and A. F. Cheng. Pathology of fatal human infection associated with avian influenza A H5N1 virus. *J. Med. Virol.*, 63(3):242–246, March 2001.

[84] T. M. Tumpey, T. R. Maines, N. Van Hoeven, L. Glaser, A. Solorzano, C. Pappas, N. J. Cox, D. E. Swayne, P. Palese, and J. M. Katz .. Garcia-Sastre. A two-amino acid change in the hemagglutinin of the 1918 influenza virus abolishes transmission. *Science*, 315:655–659, 2 February 2007.

[85] P. van den Driessche and James Watmough. Further notes on the basic reproductive number. In *Mathematical Epidemiology*, chapter 7, pages 159–178. Springer Berlin/Heidelberg, 2008.

[86] D. van Riel, V. J. Munster, E. de Wit, G. F. Rimmelzwaan, R. A.M. Fouchier, A.D.M.E. Osterhaus, and T. Kuiken. H5N1 virus attachment to lower respiratory tract. *Science*, 312(5772):399, 21 April 2006. Originally published in Science Express on 23 March 2006.

[87] H. Wan and Daniel R. Perez. Amino acid 226 in the hemagglutinin of H9N2 influenza viruses determines cell tropism and replication in human airway epithelial cells. *J. Virol.*, 81(10):5181–5191, May 2007.

[88] J. Ward, J. Thackham, K. Heymer, A. Setchi, E. Aydemir, Z. Zhang, and D. Schley. A simple mathematical model of the spread of Foot-and-Mouth Disease Virus through

epithelial cells. Technical report, 7th Mathematics in Medicine Study Group (EPSRC), 2007.

[89] World Health Organization. Avian influenza. Fact sheet, Department of Communicable Disease Surveillance and Response (CSR), World Health Organization, Revised January 2004. Available online at: http://www.who.int/csr/don/2004_01_15/en/.

[90] World Health Organization. Influenza. Fact Sheet 211, World Health Organization, Revised March 2003. Available online at: http://www.who.int/mediacentre/factsheets/fs211/.

[91] P. F. Wright and R. G. Webster. Orthomyxoviruses. In D. M. Knipe, P. M. Howley, D. E. Griffin, R. A. Lamb, M. A. Martin, B. Roizman, and S. E. Straus, editors, *Fields Virology*, volume 1, chapter 47, pages 1533–1579. Lippincott Williams & Wilkins, fourth edition, 2001.

[92] S. Yamada, Y. Suzuki, T. Suzuki, M. Q. Le, C. A. Nidom, Y. Sakai-Tagawa, Y. Muramoto, M. Ito, M. Kiso, T. Horimoto, K. Shinya, T. Sawada, M. Kiso, T. Usui, T. Murata, Y. Lin, A. Hay, L. F. Haire, D. J. Stevens, R. J. Russell, S. J. Gamblin, J. J. Skehel, and Y. Kawaoka. Hemagglutinin mutation responsible for the binding of H5N1 influenza A viruses to human-type receptors. *Nature*, 444(7117):378–382, 16 November 2006.

[93] H-L. Yen, J. R. Aldridge, A. C. M. Boon, N. A. Ilyushina, and R. Salomon. Changes in H5N1 influenza virus hemagglutinin receptor binding domain affect systemic spread. *PNAS*, 106(1):286–291, January 2009.

[94] H-L. Yen, N. A. Ilyushina, R. Salomon, E. Hoffmann, R. G. Webster, and E. A. Govorkova. Neuraminidase inhibitor-resistant recombinant A/Vietnam/1203/04 (H5N1)

influenza viruses retain their replication efficiency and pathogenicity in vitro and in vivo. *J. Virol*, 81(22):12418–12426, November 2007.

[95] R. M. Zorzenon dos Santos and S. Coutinho. Dynamics of HIV infection: A cellular automata approach. *Phys. Rev. Lett.*, 87(16):168102, 15 October 2001.